Transcriptional reactivation of the tRNA^{Ser}/tRNA^{Tyr} gene cluster in *Arabidopsis thaliana* root tip

Guillaume Hummel[1#*], Priyanka Kumari[1#], Long Wang[2], Yan-Xia Mai[2], Nan Wang[1], Negjmedin Shala[1], Emir Can Kaya[1,4], Jia-Wei Wang[2,3], Chang Liu[1*]

SHORT TITLE

Root tip reactivation of the SYY cluster

ADDRESSES

1 Department of Epigenetics, Institute of Biology, University of Hohenheim, Otto-Sander-Straße 5, 70599 Stuttgart, Baden-Württemberg, Germany

2 National Key Laboratory of Plant Molecular Genetics (NKLPMG), CAS Centre for Excellence in Molecular Plant Sciences (CEMPS), Institute of Plant Physiology and Ecology (SIPPE), Chinese Academy of Sciences (CAS), Shanghai 200032, China

3 ShanghaiTech University, Shanghai 200031, China

4 Department of Agricultural Genetic Engineering, Ayhan Şahenk Faculty of Agricultural Sciences and Technologies, Niğde Ömer Halisdemir University, Merkez Campus, 51240, Niğde, Turkey

# These authors contributed equally to this work.

***** Corresponding contacts
Hummel, Guillaume: guillaume.hummel@uni-hohenheim.de
Liu, Chang: chang.liu@uni-hohenheim.de

The authors responsible for the distribution of materials integral to the findings presented in this article, and in accordance with the policy described in the Instructions for Authors, (https://academic.oup.com/plcell/pages/General-Instructions) are: Guillaume Hummel (guillaume.hummel@uni-hohenheim.de) and Chang Liu (chang.liu@uni-hohenheim.de).

KEYWORDS

Transfer RNA, tandem repeat, chromatin, translation, root, EXTENSIN

ABSTRACT

Plants retain an exhaustive tRNA gene repertoire in their nuclear genome. How important are these individuals, how exactly plants orchestrate their usage, and for what purposes, is poorly understood. *Arabidopsis thaliana* chromosome 1 holds a cluster of tandemly repeated $tRNA^{Ser}$ and $tRNA^{Tyr}$ genes (SYY cluster). They intersect with constitutive heterochromatin and are transcriptionally silenced. Here, we resolve the tissular expression pattern of this cluster along seedling establishment. We show the root cap columella and few adjacent lateral root cap cells to be the main sources of SYY cluster tRNAs. The transcriptional reactivation of this genomic region occurs there although elevated DNA methylation levels. Furthermore, we evidence that these cells are able to accumulate high levels of a transgenic EXTENSIN rich in serine and tyrosine, and that the CRISPR/Cas9 deletion of the SYY cluster alters such phenomenon. Altogether, our work sheds light on pioneering evidence of a developmental and cell-specific expression program for a plant tRNA gene.

INTRODUCTION

Transfer RNAs (tRNAs) represent a category of small non-coding RNA species. Found in all life forms, tRNAs are evolutionarily ancient RNAs (Chan and Lowe, 2016). Their existence relates to an essential process for life: protein biosynthesis. tRNAs work as adaptor molecules that charge an amino acid at their 3’ ends, and subsequently transfer

it at the C-terminus of nascent polypeptides inside ribosomes (Hoagland et al., 1958; Berg et al., 1961; Holley et al., 1965). The fidelity of translation relies on highly conserved structural elements (Berg and Brandl, 2021; Giegé and Eriani, 2023). They ensure that tRNAs are charged with the cognate amino acid, and accurately match it with one of the 61 codons composing messenger RNAs (mRNAs) (Nirenberg et al., 1965). Therefore, a set of tRNA species exists for the decoding of each amino acid (Chan and Lowe, 2016).

The evolution of nuclear genomes went along with a complexification of tRNA gene (tDNA) contents, in terms of copy number and sequence diversity (Goodenbour and Pan, 2006; Santos and Del-Bem, 2022). tRNAs are generally represented by multigenic tDNA families from which the individuals are spotted along chromosomes (Santos and Del-Bem, 2022; Hummel and Liu, 2022). Numerous mutational events accompanied the genomic proliferation of tDNAs and diversely increased the pool of unique tRNA sequences among species (Goodenbour and Pan, 2006). Polymorphisms are either silent, or make the structure of transcripts variably diverging from a functional tRNA (Chan and Lowe, 2016). Ticketed as “tRNA-like”, these pseudo-RNAs might be impaired in expression, stability and/or their function in translation.

The copy number of a nuclear tDNAome appears positively correlated to the genome size, the content of protein-coding genes and codon frequencies (Goodenbour and Pan, 2006; Michaud et al., 2011; Santos and Del-Bem, 2022). It implies that nuclear genomes retain multiple copies of corresponding tDNAs in proportion to the presumed demand for specific amino acids, ensuring an ample supply of tRNAs to meet the requirements of protein synthesis. Nonetheless, a growing body of evidence reveals that in a given species and condition, only a restricted fraction of the nuclear tDNAome might be transcribed. Immunoprecipitations of chromatin bound by the RNA polymerase (RNAP) III machinery, and tRNA sequencing experiments, showed that roughly half of the 619 tDNAs contribute to less than 1% of the tRNA abundance in human (Moqtaderi et al., 2010; Canella et al., 2010; Oler et al., 2010; Gogakos et al., 2017; Thornlow et al., 2018; Torres, 2019). Congruent conclusions were recently stated in plants (Hummel et al., 2020; Ma et al., 2021; Liu and Sun, 2021; Hummel and Liu, 2022). Therefore, it is questionable why

eukaryotes retain so much tDNAs in their nuclear genome. Are some of them developmentally/environmentally regulated? What is the biological importance of individual tDNAs?

The nuclear genome of the plant *Arabidopsis thaliana* Col-0 consists of five chromosomes carrying 586 tDNAs (Cognat et al., 2022). While most are dispersed along arms, a subset of proline, serine and tyrosine tDNAs organize in clusters (Green and Weil, 1989; Beier et al., 1991; Theologis et al., 2000; Michaud et al., 2011; Hummel et al., 2020; Hummel and Liu, 2022). Chr1 and Chr2 comprise six small clusters (*c.a.* 3-6kbps) numbering up to 11 $tDNAs^{Pro}$ (Hummel et al., 2020; Hummel and Liu, 2022). Furthermore, Chr1 holds a large array (*c.a.* 40kbps) of 27 $tDNAs^{Ser}$ and 54 $tDNAs^{Tyr}$ tandemly repeated 27 times (Ser-Tyr1-Tyr2)$_{27}$ (Hummel et al., 2020; Hummel and Liu, 2022), which is referred in this work as the "SYY cluster". A previous work revealed that tDNA clusters stand in epigenomic environments unfavourable for RNAPIII transcription and are silent (Hummel et al., 2020). Herein, we explore the conditions, molecular mechanisms, and physiological significance of their reactivation by focusing on the SYY cluster.

RESULTS

The SYY cluster consists of a core region which expanded by tandem duplication

Out of the 20 tDNA families encountered in the Col-0 nuclear genome, $tDNA^{Tyr}$ one is the most abundant, and counts 70 genes (Cognat et al., 2022). For the sake of description, and to explore their genetic diversity and organization, we sought to hierarchize $tDNAs^{Tyr}$ based on three factors: the layout (dispersed/clustered), nucleotide polymorphisms (NPs), and gene copy numbers (**Supplemental Fig. S1, A and B**). Dispersed tDNAs are labelled "D-", and clustered ones "C-". Inspired from 5S ribosomal DNA (rDNA) work (Cloix et al., 2002), the nomenclature defines tDNA NPs represented by the highest gene copy number as "major". All others are decreasingly categorized as "minor". Thus, D-$tDNAs^{Tyr}$ comprise a MAJOR represented by 14 copies and two MINORs represented by a total of two copies.

C-tDNAs^{Tyr} comprise a MAJOR represented by 32 copies and nine MINORs represented by a total of 22 copies.

The analysis of secondary structures revealed that out of the 16 D-tDNAs^{Tyr}, only one (*i.e.,* MINOR1) leads to a tRNA-like transcript (**Supplemental Fig. S1, A and D**). By opposition, out of the 54 C-tDNAs^{Tyr}, a total of 13 MINORs (*i.e.,* 1, 5, 6, 7, 8 and 9) lead to tRNA-like RNAs (**Supplemental Fig. S1, A and E**). These pseudo-tRNAs are characterized by different structural mismatches which might be deleterious for their stability and role in translation (**Supplemental Fig. S1, D and E**). They might not pass through tRNA quality controls (Phizicky and Hopper, 2023).

tDNAs^{Met} and tDNAs^{Tyr} are the only two tDNA species containing an intron in the nuclear genome of *A. thaliana* (Michaud et al., 2011). We set up a secondary nomenclature based on the sequence of these introns (**Supplemental Fig. S1C**). D-tDNAs^{Tyr} have 12 different intron variants (VARs), while C-tDNAs^{Tyr} only have seven. Interestingly, we found a highly conserved GCAGAU motif in C-VARs (**Supplemental Fig. S1C**). The motif is also present in D-VARs 8 and 12 species. This suggests that during the history of tDNA^{Tyr} content evolution in Brassicaceae genomes, SYY cluster formation is phylogenetically linked to these two D-tDNA^{Tyr} species.

Then, we confronted the two nomenclatures to unveil the internal organization of the SYY cluster (**Supplemental Fig. S2, A to D**). We assigned to each repeat unit (1 to 27) and to each tDNA^{Tyr} cassette (Y1 and Y2) the associated MAJOR/MINOR and intron VAR (**Supplemental Fig. S2 A and B**). The resulting pattern led us to the identification of an obvious region, where the pairs of MAJOR-MAJOR concentrate. We defined it as the core region (CR). This last is flanked by variable regions in which the proportion of MINORs and tDNA-like pseudogenes increases. Besides, at one side of this cluster region, several copies in the MAJOR-MAJOR pairs are present, which we named CR*.

As a whole, the MAJOR is mainly represented by the Y2 position (*c.a.* 80%) while MINORs are preponderantly found at the Y1 cassette (*c.a.* 60%) (**Supplemental Fig. S2C**). Due to

the presence of unique sequence variations, the transcripts derived from MAJORs can be specifically probed, making it feasible to study the expression and regulation of C-tDNAs^{Tyr} in this cluster (Hummel et al., 2020).

Germination positively affects the expression of the SYY cluster

It has been previously shown that the SYY cluster forms constitutive heterochromatin (CH), and is silenced epigenetically in plants (Hummel et al., 2020). The silencing was artificially alleviated with pharmacological drug treatments, and epigenetic mutants altering the post-replicative maintenance of DNA methylation (Hummel et al., 2020). Nonetheless, the natural conditions favouring its transcription remained pending.

Developmental transitions have been pivotal in the understanding of CH dynamics (Benoit et al., 2013; Simon and Probst, 2023). Particularly, germination associates with a decompaction of CH which promotes the expression of the silent fraction of 5S rDNA clusters in *A. thaliana* cotyledons (Mathieu et al., 2003). Thence, we asked as an outset whether CH rearrangement during germination loosens the silencing of the SYY cluster. To do so, we defined six timepoints to monitor its expression (**Fig. 1A**). Covering all steps of seedling establishment, they correspond to imbibed seeds (0 days after stratification, DAS), test*ae* rupture (1DAS), endosperms rupture and radicles emergence (2DAS), cotyledons emergence and greening (3DAS), established plantlets (4DAS) and adult plants (14DAS).

Expectedly, D-tRNAs^{Tyr} accumulate during germination and remain as dominant tRNA^{Tyr} species (**Fig. 1C**). C-tRNAs^{Tyr} remain lowly detectable tRNA species but their steady-state level increases transiently in 2DAS and 3DAS plantlets (**Fig. 1C**). As an additional control, membranes were stripped and rehybridized with D-tRNAs^{Ala} probe. These species accumulate comparably between the two membranes, and comfort that D/C-tRNAs^{Tyr} patterns are not the consequence of a technical issue (**Fig. 1C**). To strengthen that result, we repeated the experiment using two others independent seed batches (**Fig. 1C**). C-tRNAs^{Tyr} were quantified from unsaturated exposures, and signals normalized based on

the RNAPI transcription-derived 5.8S rRNA quantified from Roti staining. 0DAS signals were used as references to calculate fold-changes. Results confirmed that, whatever the seed batch, C-tRNAs^{Tyr} momentarily over accumulate in 2/3DAS plantlets. Fold-changes vary between 54 and 572 for the 2DAS stage and between 76 and 382 for 3DAS stage (**Fig. 1C**). Only for seed batch #2, C-tRNAs^{Tyr} were detected in 4DAS plantlets but fold-change (34) remained lower than abovementioned (**Fig. 1C**).

Thereupon, we concluded that germination indeed has a positive effect on the expression of the SYY cluster. C-tRNAs^{Tyr} seem to follow a temporal accumulation pattern restricted to 2/3DAS plantlets. Nonetheless, the upregulation of the SYY cluster stays relatively very low compared to D-tDNAs^{Tyr} expression (**Fig. 1C**).

Root tip cells source SYY cluster transcripts during vegetative development

The accumulation dynamic of C-tRNAs^{Tyr} during germination might originate from two hypothetic scenarios. On the one hand, the chromatin of 2/3DAS plantlets might allow a light expression of the SYY cluster all over organs (“background hypothesis”). In this scenario, this ability is only gained at 2/3DAS stages, then lost. On the other hand, the chromatin of at least one tissue might allow a high expression of the SYY cluster (“dilutive hypothesis”). In this scenario, this ability is gained at 2/3DAS stages, and pertained despite the growing of other tissues/organs not expressing the SYY cluster. In other words, the developmental proportions in which the SYY cluster is activated in 2/3DAS plantlets might enable a transient enrichment of C-tRNAs^{Tyr} in RNA extracts. Later, the development of tissues/organs negative for the SYY cluster expression might progressively dilute C-tRNAs^{Tyr} by contributing their own RNAs in extracts.

To infer one of the two hypotheses, we defined an extra intermediary stage at 7DAS (**Fig. 1B**). Situated between 4 and 14DAS, the 7DAS timepoint is set just after the depletion of C-tRNAs^{Tyr} level (**Fig. 1C**). Consequently, their non-detection in 7DAS plantlets would tip in favour of the background scenario. Contrariwise, a tendentious detection in at least one part of 7DAS plantlets would advocate the dilutive scenario.

To address it, we worked out an anatomization procedure deconstructing 7DAS plantlets into their main organs, *i.e.,* plantlets (T), shoots (S), roots (R), and the lower half root parts (LR) (**Fig. 1B**). Total RNAs were extracted from T, S, R and LR segments, then northern blotted. While control D-tRNAs^{Ala} accumulate equally among the four samples, we noted a preferential enrichment of C-tRNAs^{Tyr} in R and LR RNA extracts (**Fig. 1D**). Nevertheless, they are nondetectable in T and S RNA extracts. Remarkably, their enrichment is higher in the lower root comparatively to the whole root organ (**Fig. 1D**). It suggests that a gradient expression program along the root axis governs the SYY cluster. We further dissected roots into segments containing tip and dividing cells (S3), elongating cells (S2) and differentiating cells (S1) (**Fig. 1B**). Northern blotting their RNA extracts showed that C-tRNAs^{Tyr} increasingly accumulated from S1 to S3, but control D-tRNAs^{Ala} accumulate homogeneously (**Fig. 1D**). Altogether, these results credit the dilutive hypothesis and disclose that at least one tissue located in the root tip or in the mitosis zone abundantly accumulate C-tRNAs^{Tyr} during the vegetative development of *A. thaliana*.

The SYY cluster is indeed the genomic region producing C-tRNAs^{Tyr} in roots

To ascertain that the SYY cluster is the genomic region responsible for the accumulation pattern of C-tRNAs^{Tyr} in roots, knock-out mutants bearing the deletion of this region were produced with the CRISPR/Cas9 technology (**Fig. 2, A and B**). The absence of the SYY cluster in independent lines, referred herein to as *syy-1* and *syy-2*, was confirmed by PCR and sequencing (**Fig. 2, C-E and Supplemental Dataset 1**).

Contrarily to Col-0, *syy-1* and *syy-2* roots showed only a faint C-tRNAs^{Tyr} signal, which we considered as cross-hybridization background (**Fig. 2F**), This experiment clearly demonstrates that the SYY cluster produces C-tRNAs^{Tyr} in our seed's genome, and is responsible for the developmental expression pattern in root. D-tRNAs^{Tyr} accumulate comparably between the three genotypes as well (**Fig. 2F**), suggesting that the transcription and regulation of D/C-tDNAs^{Tyr} is completely dissociated.

C-tDNAs^{Tyr} are strongly expressed in roots when not in a tandem repeat context

The functionality of C-tDNAs^{Tyr} gene structure was only deduced from the analysis of their *cis*-motifs, but lacked an experimental validation *in vivo* (Hummel et al., 2020). Therefore, we took the advantage of CRISPR/Cas9 lines lacking the SYY cluster to reintroduce back transgenic C-tDNAs^{Tyr} and study their transcription. We either cloned the first repeat unit in upstream of the SYY cluster (1xSYY), or engineered a C-tDNA^{Tyr} for strong expression (Ing-Y) (**Fig. 2G**). The latter contains the MAJOR sequence and the C-VAR2 intron (most represented in the SYY cluster), combined to the promoter and terminator of a D-tDNA^{Tyr} (AT5G61835) bearing all *cis*-elements required for a strong transcription of plant nuclear tDNAs (**Figs. 2G, S1B and S1C**) (Yukawa et al., 2000; Michaud et al., 2011).

Constructs were stably agrotransformed in the *syy-1* background and single insertion lines were selected in T2. For both types of the transgene, we found that reintroducing a single copy back into *syy-1* plants generates more C-tRNAs^{Tyr} than 34 genes of the SYY cluster in Col-0 roots (**Fig. 2H**). Hence, when C-tDNAs^{Tyr} are not in tandem, they have the ability to be constitutively and strongly expressed in the whole root organ. These results indicate that despite being silenced *in vivo*, C-tDNAs^{Tyr} are functional gene loci.

Columella and border cells are the main expression sites of the SYY cluster

In Col-0, root is the principal organ hosting the expression of the SYY cluster during vegetative development (**Fig. 1D**). Such finding mirrors a previous investigation showing that, among different developmental stages and organs, roots are preponderant sites of minor 5S rRNAs accumulation (Mathieu et al., 2003). The segmentation analysis we did clarifies that the average C-tRNAs^{Tyr} amount detected in the whole root is preferentially yielded by the S3 segment containing the tip and cells in mitosis (**Fig. 1, B and D**). Considering that one locus of the SYY cluster has the potential for a high and ubiquitous transcription, the reactivation of 34 C-tDNAs^{Tyr} in the S3 segment might be represented by a limited number of cells (**Fig. 2, G and H**).

To identify them, we applied a whole-mount *in situ* hybridization (WISH) strategy coupled with tyramide signal amplification (TSA) to study the distribution of C-tRNAs^{Tyr} transcripts in 4DAS root tissues (Andras et al., 2001; Wójcik et al., 2018). Such stage was preferred because the elongation of rootlets is advanced enough to distinguish the three segments S1-3 but the entire organs tiny enough to not mingle between each other along the procedure. Positioned just after the drop of C-tRNAs^{Tyr} during germination (**Fig. 1C**) the 4DAS stage also suits to further legit the dilutive hypothesis with this tissular analysis. In concert with **Figs. 2F and H**, the *syy-1* deletion allele was used as negative control.

The WISH experiments generated a staining pattern consistent with that from our northern blot assays, in which the signal intensity progressively increased from S1 to S3 (**Fig. 3A**). The counter-lighting made evident that the halo progression is homogenous within S2 and S3 (**Fig. 3A**). Thus, the tissular identity is not the main biological parameter for the establishment of this gradient but more the fact that cells are dividing and not fully differentiated. Nevertheless, the four peripheral cells of the columella (RCC1-4), and few adjacent border cells (LRC), were systematically subject to a staining higher than dividing cells (**Fig. 3B**) (Dolan et al., 1993). Hotspots of C-tRNAs^{Tyr} accumulation, RCC and LRC cells might contribute to their high enrichment in the S3 segment and represent an evident case of cell-specific expression (**Fig. 1D**). As expected, *syy-1* rootlets didn't exhibit the staining (**Fig. 3, A and B**).

High DNA methylation levels accompanies natural SYY expression in roots

Knowing that the SYY cluster reactivates along Col-0 roots, we sought to decipher how it relates to changes in its methylation landscape. Indeed, DNA methylation is an epigenetic mark taking part in SYY cluster silencing (Hummel et al., 2020). Methylation-sensitive restriction enzymes (MSREs), and bisulfite sequencing datamining, were used to that end.

The alignment of C-tDNA^{Tyr} sequences led to the identification of MSRE sites for the three methylation sequence contexts: *Bsp119I* (TTCGAA) for mCGs, *MspI* (CCGG) for mCHGs, and *HpyF3I* (CTNAG) for mCHHs (**Supplemental Dataset 2 and Supplemental Fig. S3,**

A and B). An unmethylated D-tDNA^{Val} (AT3G11395) possessing all these sites was used as a positive digestion control (**Supplemental Dataset 2 and Supplemental Fig. S3, A and B**).

Upon enzymatic treatment in the three methylation contexts, the Val control is not amplified (**Supplemental Fig. S3, C and D**). It ascertains that this locus is unmethylated, and that input DNA is fully digested. On the contrary, wild-type Y1 and Y2 loci resist *Bsp119I* and *MspI* treatments, and were amplified (**Supplemental Fig. S3, C and D**), confirming these genes to be predominantly CG and CHG methylated in Col-0 roots. However, Col-0 Y1 and Y2 genes did not resist *HpyF3I* treatment, and were only weakly amplified (**Supplemental Fig. S3, C and D**). It shows that they are only barely CHH methylated, what is a common trait of the *A. thaliana* methylation landscape (Law and Jacobsen, 2010; Zhang et al., 2018). Chop-PCR amplifications using *ddm1* template DNA revealed enhanced Y1 and Y2 sensitivities to digestions. It substantiated that the MSRE design detects significant DNA hypomethylations in CG (Y1 and 2) and in CHG (Y2) (**Supplemental Fig. S3, C and D**). Y1 amplifications remain high and persistent for the CHG context whatever the genotype (**Supplemental Fig. S3, C and D**). The bias comes from 12 MINORs not holding the *MspI* site, and mainly standing at the Y1 position (**Supplemental Figs. S2A, S3A and B**). No significant changes in mCHH levels were observed between Col-0 and *ddm1* with this technique (**Supplemental Fig. S3, C and D**).

To verify that DNA methylation dynamics at chosen chop-PCR sites reflect what happens for the entire cassette, Col-0 and *ddm1* root methylomes were reanalysed (Zemach et al., 2013). Because the SYY cluster is highly repetitive, using TAIR10 reference would undeniably distort interpretation of DNA methylation levels at genes with identical sequences. To bypass the issue, we edited a new reference REF1 wherein the SYY cluster was replaced by a consensus (**Supplemental Dataset 3 and Fig. S3E**). In this last, each position represented by more than one nucleotide upon alignment was considered as degenerated (N). Y1 and Y2 tDNA sequences were both blocked with the MAJOR to correlate DNA methylation dynamics with northern blot analysis. Introns i1 and i2 were however kept consensual and are by chance different (**Supplemental Dataset 3**

and Fig. S3E). Overall, such design allowed us to confidently assess MAJOR methylation status at Y1 and Y2 cassettes.

Our analysis confirmed that S, Y1, and Y2 cassettes are predominantly methylated (mCG > mCHG > mCHH) (**Supplemental Fig. S3F**). In *ddm1*, CG and CHG hypomethylations were observed, while mCHHs were unchanged. This dynamic associates with an alteration of the SYY cluster expression pattern in root, which becomes overexpressed in the three segments (**Fig. 1D**). Contrastingly, the triple knock-out mutant for active demethylases REPRESSOR OF SILENCING 1, DEMETER-LIKE 2, and 3 (*rdd*) has no effect (**Fig. 1D**). Therefore, natural SYY cluster expression might likely result from the modulation of DNA methylation maintenance mechanisms.

Surprisingly, the two methods established that the gradient SYY cluster expression in Col-0 roots occurs despite no significant changes in DNA methylation levels among the three segments S1-3 (**Figs. 1D and 4A-B**). The results contrast with the strong and constitutive expression of the transgenic 1xSYY repeat in the absence of DNA methylation, and mimicking *ddm1* effect (**Figs. 1D, 2G-H, S3A-F and 4C**). The reanalysis of published bisulfite sequencing data also showed no DNA hypomethylation in root tip tissues, including columella (**Figs. 4D** and **S4**) (Kawakatsu et al., 2016). Instead, high C-tRNAs^{Tyr} accumulation in this tissue correlates with a *de novo* hypermethylation of S, Y1 and Y2 cassettes caused by the RNA-directed DNA methylation pathway (RdDM) (**Figs. 3A-B and 4D**) (Kawakatsu et al., 2016; Zhang et al., 2018). RdDM is mediated by RNAPIV and V, the activity of which thus coincides with C-tRNAs^{Tyr} enrichment in S3 (**Figs. 1D and 4D**). Hence, we wondered whether SYY cluster expression in roots could be an RdDM by-products. Indeed, RNAPV RNAs could largely host a tRNA precursor due to their size variations (Böhmdorfer et al., 2016). Nevertheless, knock-out mutants for RNAPIV- and V-specific subunits (*i.e., nrpd1* and *nrpde1*) have no effects on C-tRNAs^{Tyr} accumulation in S3 (**Fig. 1D**). By contrast, the knock-down *nrpc7* mutant leads to decreased C-tRNAs^{Tyr} and D-tRNAs^{Ala} in S3 (**Fig. 1D**). It comforts that the SYY cluster is expressed via a classical RNAPIII transcriptional system in the root tip.

The hypomethylated SYY cluster is transcribed at the nuclear periphery in *ddm1*

To have more insights on the molecular dynamics accompanying SYY cluster reactivation, sequencing data of transposase-accessible chromatin (ATAC-seq) were remapped using the REF1 (Zhong et al., 2021). Interestingly, nucleosomes repositioning in *ddm1* mediates a preferential chromatin accessibility of the Y2 cassette, where the MAJOR is mainly represented (**Supplemental Figs. S2D and S5A**). ATAC-seq peaks remain however low and narrow at C-tDNAs in *ddm1* (max 150) when compared to D-tDNAs of Ala and Tyr families. Indeed, the ATAC-seq value at their mean coordinate can fluctuate between 150 and 2000 (**Supplemental Fig. S5B**). Moreover, ATAC-seq peaks typically follows a broad gaussian-like distribution wherein the max is axed on the D-tDNA (**Supplemental Fig. S5C-D**). This could mean that the absence of DDM1 either trigger a low and homogenous accessibility of the Y2 locus, or the high accessibility of few MAJORs smoothed by the average.

The fluorescence *in situ* hybridization (FISH) of the SYY cluster in the nuclei of Col-0 total roots disclosed its presence at the nuclear periphery (**Supplemental Fig. S6**). The result is in line with the enrichment of heterochromatin at this subnuclear location in *A. thaliana*, and the reanalysis of chromatin immunoprecipitation data revealing contacts between the SYY cluster and lamina-like protein CROWDED NUCLEI 1 (Santos et al., 2020; Hummel and Liu, 2022). No 3D translocation of the SYY cluster was noticed by FISH in *ddm1* nuclei (**Supplemental Figs. S6**). Besides, no FISH signal was detected in *syy-1* and *syy-2* root nuclei, thus confirming the deletion at the cytogenetic level.

The linkup of above data suggests that the reactivation of the hypomethylated SYY cluster in *ddm1* occurs in association with the nuclear periphery, without dramatic reorganization of its own chromatin, and with a preferential transcription of the Y2 locus.

Root tip cells are compatible with high Ser, Tyr, and Pro translational demands

Corroborating amino acid frequencies in gene coding sequences with tDNA copy numbers showed that C-tDNAs are excessive copies (Michaud et al., 2011; Hummel et al., 2020). It signifies that the expression of D-tDNAs theoretically produces tRNA amounts sufficient to translate the putative mRNA pool encoded in the *A. thaliana* genome.

Therefore, the existence of excessive tDNAs, for instance those in the SYY cluster, might hint a translatome demanding on high levels of the corresponding Ser, Tyr in certain cells or developmental phases. Following this logic, we datamined *A. thaliana* genome for proteins rich in these amino acids. This analysis pointed out a subset of proteins outlying *A. thaliana* proteome and co-enriched in Ser, Tyr and Pro (**Fig. 5A**). EXTENSINs (EXTs) 22, 6, 9, 18 and 19 are in the top five (**Fig. 5A and Supplemental Dataset 4**). EXTs belong to a larger superfamily (*c.a.* 166 genes) of cell wall and secreted components named hydroxyproline-rich glycoproteins or HRGPs (Showalter, 1993; Showalter et al., 2010; Hijazi et al., 2014; Castilleux et al., 2018; Driouich et al., 2021; Moussu and Ingram, 2023). The primary sequence of dicot EXTs consists in the tandem repetition of a low-complexity motif containing stretches of Pro plus Ser, Tyr, and few other residues (**Supplemental Dataset 4**) (Showalter, 1993; Showalter et al., 2010).

To decrypt how plants manage high Ser, Tyr and Pro translational demands, we designed a reporter construct (RC) forcing the strong and constitutive expression of the EXT19 coding sequence fused to the GFP (**Fig. 5B**). The constitutive UBIQUITIN10 promoter and its intron-containing 5'UTR lead to a constant transgene expression in all tissues, and were used (Norris et al., 1993; Sun and Callis, 1997) (**Fig. 5B**). To hinder the integration of the heterologous protein in the cell wall, the putative N-ter secretion signal of the EXT19 was removed and antagonized by a NLS tag in C-ter of the construct (**Fig. 5B**). The cytoplasmic retention of the protein was preferred to purify it without highly destructive methods. The fluorescent tag was intentionally put in C-ter of the construct, so the pre-requisite for its accumulation is a prior translation of the Ser, Tyr, and Pro-rich cassette. However, an internal initiator methionine was kept at the GFP tag.

The RC was stably agrotransformed in the Col-0 background, and the accumulation of the fusion protein scrutinized at the tissular level in defined germination timepoints (**Fig. 1A**). In the wild-type background, a strong accumulation of EXT19-GFP-NLS was observed in whole 0DAS embryos (**Supplemental Fig. S7A, B and M**). The developmental stage validated that RC mRNAs can be ubiquitously expressed and translated. Starting from 1DAS and maintained till the adult 14DAS stage, the constitutive accumulation of EXT19-GFP-NLS in roots is cleared in favour of a cell-specific expression in the four peripheral RCC and adjacent LRC cells (**Figs. S7C-M and 5C-D**). Interestingly, protein level progressively increases from the first layer of cells (immediately below the meristem) to the peripheral one in detachment (**Fig. 5D**). Thus, RC expression follows a spatiotemporal logic in these tissues related to the maturation and specialization of RCC and LRC cells. Parallelly, EXT19-GFP-NLS accumulation gradually declines with cotyledons growth, and was not detected in adult leaves (**Supplemental Fig. S7A-M**). No signal was detected in untransformed plants using identical settings (**Supplemental Fig. S7A-M**).

The homeostasis of columella and lateral root cap tissues is compatible with a continuous translation and stabilization of the overexpressed EXT19-GFP-NLS along seedling establishment. It hints that the tissues are physiologically specialized to elaborate Ser, Tyr, and Pro-rich translatomes. Noticeably, major C-tRNAs^{Tyr} and EXT19-GFP-NLS co-enrichment in the S3 segment, RCC, and LRC cells suggests that the SYY cluster is a genomic region involved in this tissular peculiarity by the production of tRNA amounts favouring translation (**Figs. 1D, 3A-B, S7A-M, and 5C-D**).

SYY cluster tRNAs boost the translation of a transgenic EXTENSIN in the root tip

Next, we performed a genetic cross to bring the RC into *syy-1* plants to examine how the EXT19-GFP-NLS protein synthesis can be influenced by the absence of the SYY cluster. We found that the SYY cluster deletion correlates with a significant decrease of GFP fluorescence in *syy-1* RC lines (**Fig. 6A-B**). It demonstrates that the expression of the SYY cluster indeed results in tRNA amounts potentializing translation in the candidate tissues. To further rule out the possibility that *syy-1* impaired EXT19-GFP-NLS at a

transcriptional level, we brought an additional reporter construct (RC control), in which EXT19-GFP was replaced by mCherry, into these plants with RC. We observed that the mCherry-NLS proteins accumulated in the nucleus of all root cells with similar abundance in wild-type and *syy-1*, but EXT19-GFP-NLS clearly showed impaired protein accumulation in *syy-1* (**Supplemental Fig. S8**). It comforts that transgenes transcription was not affected in *syy-1*.

EXT19-GFP-NLS was also western blotted in Col-0 (negative control), Col-0 RC and *syy-1* RC root protein extracts (**Fig. 6C**). A protein around 100KDa, corresponding to EXT19-GFP-NLS, was specifically detected in RC lines (**Fig. 6C**). Downregulated in *syy-1* protein extract, its behaviour reflects what observed for the root tip fluorescence (**Fig. 6A-B**). Surprisingly, an enhanced accumulation of shorter translation products is detected in the *syy-1* extract (**Fig. 6C**). Recognized by the antibody, they might result from alternative initiation of translation at internal methionines and in phase with the GFP sequence. tRNA shortage in *syy-1* background might slow down or pause ribosomes on EXT19 coding sequence, thus promoting such phenomenon. The presence of these products further comforts that the difference in the EXT19-GFP-NLS accumulation between Col-0 and *syy-1* is not due to an RNA silencing mechanism.

DISCUSSION

Representing *c.a.* 16% of total RNAs, tRNAs are the second most abundant RNA species in the cell after rRNAs (Walbot, 1972). It might have contributed to define them very early as “housekeeping” RNAs. One of the oldest academic origin of such designation is traced back to the end-70’s, when Rifkind and colleagues worked on the role of erythropoietin in cell differentiation (Rifkind et al., 1976). Nevertheless, the qualifier led to a misconception that tRNA expression might be statically high and ubiquitous to make sure their amount is not a limiting factor in translation (Hummel et al., 2019).

Hereinabove, we support that a subset of $tRNA^{Tyr}$ genes, tandemly organized with $tRNA^{Ser}$ ones in a genomic structure called SYY cluster, is subject to a developmental expression

pattern along root. Cell layers bordering protective tissues of the meristem *i.e.,* columella and lateral root cap (Dolan et al., 1993), are the main transcriptional hotspots of the SYY cluster during seedling establishment. Our work reinforces growing experimental manifestations that the tRNAome is highly dynamic. Digging into the sequence diversity of species encompassing the 16% tRNAs (*i.e.,* isodecoder tRNAs) evidenced that: i) only few of the redundant tRNA loci inserted in a nuclear genome are expressed in a given condition and, ii) the unequal contribution is dynamically reshaped upon developmental and environmental factors (Moqtaderi et al., 2010; Canella et al., 2010; Oler et al., 2010; Gogakos et al., 2017; Thornlow et al., 2018; Torres, 2019; Torres et al., 2019; Hummel et al., 2019, 2020; Ma et al., 2021; Liu and Sun, 2021; Hummel and Liu, 2022).

Recently, the expression and roles of individual $tRNA^{Phe}$ genes was investigated in mouse (Hughes et al., 2023). Three isodecoder $tRNA^{Phe}$ species exist in mouse nuclear genome. They are represented by seven genes: Phe-1-1, -1-2, -1-3, -1-4, plus -1-5 for the first, and -2-1, -3-1 for the two others (Hughes et al., 2023). The seven are characterized by distinct chromatin accessibilities in and between organs, but similar RNAPIII occupancies except Phe-2-1 which seems poorly accessible and transcribed (Hughes et al., 2023). Similar to our design, authors resorted a CRISPR/Cas9 approach to individually or combinatorically knock-out $tRNA^{Phe}$ loci. This approach interestingly demonstrated that Phe-1-1 expression significantly contributes to brain, liver and spleen $tRNA^{Phe}$ accumulations while Phe-1-2 in spleen, and Phe-3-1 in brain and liver (Hughes et al., 2023). Their inactivation occasions wide transcriptional plus translational reprogramming in these organs. Phe-1-1 knock-out leads to neuronal and behavioural alterations (Hughes et al., 2023). Moreover, disrupting one $tRNA^{Phe}$ gene triggers a transcriptional adaptation of others which doesn't rescue the translational defects and induces amino acid misincorporations (Hughes et al., 2023). Also authors feature that the expression of at least six of $tRNA^{Phe}$ genes is required for a normal embryo development, the knock-out of Phe-1-1 having the most dramatic effects (Hughes et al., 2023). Likewise *A. thaliana*, tRNA loci are scattered in the genome of most bacteria, but a subset is organized in long arrays named L-arrays (Santamaría-Gómez et al., 2021). Usually lowly expressed, authors show the L-array of *Anabaena* sp. PCC 7120 is turned on under translational stress and contributes to survival (Santamaría-Gómez et al., 2021).

A partition between stable and inducible tRNA genes therefore already exists in the regulatory toolbox of primitive organisms.

In this work, we evidence that the gradient expression of the SYY cluster along root occurs despite elevated CG methylation levels. Its behaviour strikingly tallies the one of 5S rRNA gene clusters, tandem repeats of which are also transcribed by RNAPIII despite elevated CG methylation levels in *A. thaliana* (Mathieu et al., 2002). The constatation contrasts with the previous work, thereby it was showed that CG methylation is involved in the silencing of clustered $tRNA^{Tyr}$ genes (Hummel et al., 2020). The strong and constitutive expression of the transgenic SYY repeat further comforted the negative impact of high DNA methylation levels on tRNA genes transcription. Same conclusions were drawn in *Xenopus laevis* oocytes, where the injection of an artificially methylated $tRNA^{Lys}$ gene inhibited at 80% its transcription (Besser et al., 1990). Transcribing artificially methylated 5S rRNA genes was however doable *in vivo* and *in vitro* (Besser et al., 1990; Mathieu et al., 2002).

tRNA and 5S rRNA gene transcriptions do not involve the same RNAPIII promoters and pioneering factors. tRNA genes are characterized by a type 2 promoter and relies on sequential interactions between TFIIIC, TFIIIB and RNAPIII (Roeder, 2019). 5S rRNA genes have a type 1 promoter, and require the additional transcription factor TFIIIA sequentially recruiting TFIIIC, TFIIIB and RNAPIII (Roeder, 2019). Therefore, 5S rRNA gene transcriptional insensitivity to DNA methylation might be explained by a more tolerant pre-initiation complex assembly mediated by TFIIIA binding pattern. This hypothesis is however refuted as TFIIIC and B can bind methylated type 2-like promoters, and several tRNA/Alu-related short interspersed nuclear elements (SINEs) are expressed despite high DNA methylation levels in human cells (Varshney et al., 2015). The alteration of their methylation landscape with methyltransferases knock-out, or 5-azacytidine treatments, doesn’t stimulate their expression but reactivates silent protein coding genes (Varshney et al., 2015). Instead, authors show that histone methylations (*i.e.,* H3K9me3) primarily inhibit RNAPIII transcription at SINEs (Varshney et al., 2015). In parallel, Sizer and colleagues exemplifies several TFIIIC, TFIIIB and RNAPIII-bound tRNA genes located in

CpG islands (Sizer et al., 2022). Furthermore, *C. elegans* TFIIIC pauses independently of RNAPIII recruitment at repetitive tRNA-like pseudogenes and SINEs enriched in H3K9me2, an heterochromatic mark found in the SYY cluster (Stutzman, et al., 2020; Hummel et al., 2020; Hummel and Liu, 2022). TFIIIC “extra-sites” interact with the lamin-associated protein LEM2 at the nuclear periphery (Stutzman, et al., 2020). It mirrors interactions between the SYY cluster and CRWN1 (Hummel and Liu, 2022), and its location in the same subnuclear domain as revealed by our FISH.

Thence, DNA methylation might not be the main silencer of the SYY cluster. In *ddm1* and *met1* rosettes, or in 5-azacytidine/zebularine-treated plants, $tRNA^{Tyr}$ quantities produced by 34 clustered loci remain low relatively to the expression of 16 dispersed ones (Hummel et al., 2020). Alleviating DNA methylation has no impacts on the silencing of $tRNA^{Pro}$ gene clusters (Hummel et al., 2020). While DNA methylation profile at the SYY cluster doesn’t change along root, the compaction of nucleosomes as their composition in histone variants might be more dynamic parameters during development (Rosa et al., 2014; Zhang et al., 2021; Probst et al., 2020; Probst, 2022; Feng et al., 2022; Simon and Probst, 2023). Around 150bps, the size of tRNA genes is subnucleosomal. Therefore, their expression might be particularly influenced by nucleosome positioning and chromatin compaction. Transcribed tRNA genes are generally nucleosome-free (Shukla and Bhargava, 2018). In yeast, antisense RNAPII activity at tRNA genes triggers the acetylation of histones, and sets a nucleosome-free environment potentializing RNAPIII transcription (Yague-Sanz et al., 2023). Correlating the expression of the SYY cluster in different histone mutants with its DNA methylation level will allow answering the question.

The high clustered $tRNAs^{Tyr}$ accumulation in columella and lateral root cap independently confirms that chromatin characteristics of these tissues enable the expression of repeats (Kawakatsu et al., 2016). A heterologous DDM1:GFP protein expressed under the control of native promoter accumulates in all root tissues except columella and lateral root cap in *ddm1* (Kawakatsu et al., 2016). DDM1 acts as chromatin remodeler displacing linker H1, allowing access to DNA for methyltransferases MET1 and CHROMOMETHYLATES 2 and 3 (Zemach et al., 2013). DDM1 is also responsible for the deposition of the histone variant

H2A.W at heterochromatin (Osakabe et al., 2021, 2023). H1 and H2A.W together promote the compaction of constitutive heterochromatin (Bourguet et al., 2021). The double mutant *h1 h2a.w* leads to a strong decompaction, and occasions the *de novo* methylation of heterochromatin via the RdDM pathway (Bourguet et al., 2021). Interestingly, columella cells are characterized by downregulated H1.1, H1.2, H2A.W6 and H2A.W7 mRNA levels, and a global RdDM-mediated genome hypermethylation in CHH (Kawakatsu et al., 2016). The situation strikingly phenocopies *h1 h2a.w*, and might reflect a decondensed nucleosome state favourable to the SYY cluster transcription despite a preserved maintenance of CG methylation. However, we cannot exclude that a DNA methylation dynamic internal to the SYY cluster occurs in the root tip and leads to the hypomethylation of few copies, thus promoting their deheterochromatinization and strong transcription. Recent improvements in long read sequencing will allow to go beyond this frontier at the cell-type level (Rabanal et al., 2022; Wlodzimierz et al., 2023; Fultz et al., 2023).

A comment should be made on the internal organization of the SYY cluster. Our analysis of $tDNA^{Tyr}$ variants arrangement disclosed a high selection pressure on MAJOR sequence in the core region while up and downstream regions afford more minors and pseudogenes. Therefrom, it becomes questionable whether a preferential transcription of the core region is at the basis of this selection pressure.

Our data show that columella and lateral root cap cell physiology authorizes a continuous translation and accumulation of a transgenic Ser, Tyr and Pro-rich EXTENSIN. We evidence a perfect match between the expression of the SYY cluster and the protein. SYY cluster deletion hinders the capability of such cells to produce the EXTENSIN. Our study mirrors the appealing case of *Bombyx mori* silk glands. Specific $tRNA^{Ala}$, $tRNA^{Gly}$ and $tRNA^{Ser}$ species are upregulated in the organ and confer a translational specialization for the high production of fibroin during the secretion phase (Garel et al., 1973; Siddiqui and Chen, 1975; Majima et al., 1975; Chevallier and Garel, 1982). Alike EXTENSINs, the fibroin consists in the tandem repetition of an Ala, Ser, and Gly-rich motif (Manning and Gage, 1978; Gage and Manning, 1980). Alike the SYY cluster, loci producing silk gland-specific $tRNAs^{Ala}$ are tandemly repeated (Underwood et al., 1988). The upregulation of

some $tRNA^{Gly}$ gene members in the silk gland might come from nucleosome displacements (Parthasarthy and Gopinathan, 2005).

In a future study, it will be crucial to understand the role of the SYY cluster in desquamating columella and lateral root cap cells, particularly knowing their specialization in secreting a mucilage rich in EXTENSINs and others hydroxyproline-rich glycoproteins and having profound effects on plant-microorganism interactions (Castilleux et al., 2018; Driouich et al., 2021).

METHODS

Plant material and growth conditions

Col-0 (Wild-type), *ddm1-1* (Vongs et al., 1993), *ddm1-10* (SALK_093009), *ros1-3 dml2-1 dml3-1* (Penterman et al., 2007), *nrpc7-1* (Johnson et al., 2016), *nrpd1-3* (SALK _128428) and *nrpe1-11* (SALK_029919) mutants were used in this study. Seeds were surface-sterilized for 15min in 70% ethanol, 1% Tween-20, and twice for 2min in 100% ethanol. They were sown on a half-strength Murashige and Skoog medium pH5.7 (M0255, Duchefa Biochemie) supplemented with 1% sucrose and 0.6% phytagel (Sigma-Aldrich). Seeds were stratified for 48h at 4°C, and vertically grown at 21°C on a CS 250/300_5_3 (Photon Systems Instruments) cultivation shelf equipped with LEDs (intensity: 100µmol.m^{-2}.s^{-1}, photoperiod: 16h).

Total genomic DNA extraction and sequencing

gDNA was prepared according to (Michiels et al., 2003). Sequencing of vectors, and deletion zone PCR products was performed by Eurofins Genomics.

Cloning

Dual and multiplexed CRISPR/Cas9 plasmids were obtained as described in (Wu et al., 2018; Zhang et al., 2016). To obtain the Ser/Tyr-rich reporter construct, the UBIQUITIN10 (AT4G05320) promoter and intron-containing 5'UTR, and the EXTENSIN19 (AT1G26240) coding sequence excluding the N-terminal secretion motif and stop codon were amplified from Col-0 gDNA. They were Gibson assembled, together with a GFP-NLS cassette, in a pGREEN-IIS destination vector (Hellens et al., 2000) carrying the Rubisco small subunit (rbcs) terminator, and conferring spectinomycin (bacteria) and Basta (plant) resistances (see pFK-206 in MPI for Biology Tübingen vector list). A double glycine spacer was placed between EXT19 and GFP-NLS genes. The control reporter construct was obtained identically, except that the EXT19-GFP-NLS region was replaced by a mCherry-NLS. The engineered $tRNA^{Tyr}$ locus was produced as gene strands by Eurofins Genomics, and the SYY cluster repeat was amplified from Col-0 gDNA. They were individually cloned into a pFK-206 plasmid by Gibson assembly. A mCherry gene expressed under the control of the seed-specific 2S3 promoter was used as selection marker.

Semi-quantitative chop-PCR

For each reaction, 10ng of gDNA were digested for 30min at 37°C in a 10µl mix containing 0.2µl of either Fast Digest (FD) *Bsp119I*, *MspI*, FD *HpyF3I* (Thermo Scientific enzymes), and 1µl of appropriate buffer. Reactions were inactivated for 20min at 80°C, and digested gDNA was isolated with 5V of SPRI beads (Beckman Coulter). After a 10min incubation, beads were sedimented with a magnetic stand, and supernatants removed. Beads were cleaned twice in 80% ethanol and air-dried. Elution was done in 10µl of 10nM Tris pH8.0. For each PCR amplification, 1.5µl were used as template with the ALLin™ HiFi DNA Polymerase kit (HighQu). Then, 2µl of 6x DNA loading dye (Thermo Scientific) were added, and samples were run along with a GeneRuler 1kb plus DNA ladder (Thermo Scientific), in a 1% agarose gel containing 0.05µl/ml ROTI GelStain (Carl Roth). Amplification products were analysed with a Vilber QUANTUM CX5.

Isolation of nuclei and fluorescent *in situ* hybridization

Total nuclei were extracted and sorted using a S3e Cell Sorter (Bio-Rad) as delineated in (Zhu et al., 2017; Wang et al., 2021). FISH experiments were realized with 2C nuclei, and the BAC F9K23 (GenBank: AC082643) as explained in (Montgomery et al., 2022).

Total RNA extraction

For germination time-courses, a protocol yielding in high-quality total RNAs (Chang et al., 1993) was used. For others experiments, RNAs were directly TRIzol-chloroform extracted. Concentration and quality were determined with a DeNovix DS-11 FX+.

Northern blotting

RNAs were routinely loaded in a gel consisting of 15% acrylamide/bis-acrylamide (19/1), 7M urea and 1x TBE, and resolved by electrophoresis at 150V constant in 1x TBE. RNA integrity was checked with ROTI GelStain. Then, RNAs were electrotransfered onto a Hybond-N+ nylon membrane (Amersham) for 75min at 300mA constant and 4°C in 0.5x TBE. RNA crosslinking was performed with an UVLink 1000 Crosslinker (AnalytikJena, energy mode, 2 x 120mJ/cm^2). Probes were hybridized overnight at 55°C in 6x SSC, 0.5% SDS, and at a final concentration of 20nM. Washings were performed twice in 2x SSC for 10min at 55°C, once in 2x SSC, 0.1% SDS for 30min at 55°C, and for 10min at 25°C. Then, the membrane was rotated for 1h at 25°C in 2x SSC, 0.1% SDS supplemented with 1:15000 (v/v) HRP-Streptavidin (Abcam), and washed three times in 2x SSC, 0.1% SDS for 10min at 25°C. Probes were detected with sensitive HRP substrates (Takara), and an iBrightTM CL750 Imaging System.

Whole-mount *in situ* hybridization coupled to tyramide signal amplification

The WISH procedure was essentially executed as described in (Wójcik et al., 2018), with adjustments. The material was fixed for 3h in 3.7% formaldehyde, and permeabilized for 90min at 37°C in 75µg/ml proteinase K. The material was hybridized for 16h at 37°C with 100nM probe, and washed three times for 10min at 37°C in 2x SSC, then twice for 30min

at 42°C in 2x SSC, 0.1% SDS, and three times for 10min in 1x PBS. For the TSA procedure, endogenous peroxidases were first quenched by incubating the material for 1h in a peroxidase suppressor solution (Thermo Scientific). After six baths of 5min in 1x PBS, and one of 5min in 1x PBS, 0.1% Tween 20 (PBST) at 25°C, samples were incubated for 1h at 25°C in 1x PBST, 1:15000 (v/v) HRP-Streptavidin. Upon six baths of 5min in 1x PBST, samples were incubated for 1h in 1:50 of a digoxigenin-tyramide signal amplification solution (TSA Plus DIG, PerkinElmer) prepared according to manufacturer instructions. After being washed 6x for 5min in 1x PBST, and once for 30min in 1x PBST, 5% BSA, samples were incubated overnight at 4°C in 1x PBST, 5% BSA, 1:2500 anti-digoxigenin antibodies fused to the alkaline phosphatase (Roche). Washings were performed twice for 30min in 1x PBST, 5% BSA and three times for 10min in 1x PBST. Samples were then incubated three times for 5min with 1x TNM buffer [100mM Tris pH9.5, 100mM NaCl, 50mM $MgCl_2$], and staining was performed in 1x TNM supplied with 1:50 NBT/BCIP (Roche). The reaction was finally quenched with three baths of 5min in 1x TE buffer.

Western blotting

Proteins were TRIzol-chloroform extracted and resuspended in a buffer containing 4.4M urea, 11% glycerol, 88mM Tris-HCl pH6.8, 2.2% SDS, and supplied with 10mM DTT. Proteins were stacked in 6% acrylamide/bis-acrylamide (37.5/1), 125mM Tris-HCl pH6.8 and 0.1% SDS, then resolved in 12% acrylamide/bis-acrylamide, 380mM Tris-HCl pH8.8 and 0.1% SDS. Electrophoresis was performed at 30mA constant, in 25mM Tris, 200mM glycine and 0.1% SDS. Proteins were electrotransfered onto a PVDF membrane (Immobilon-P) preactivated in methanol, at 4°C and 80mA constant for 45min. Proteins were stained in 0.1% Coomassie blue, 7% acetic acid, 50% methanol, washed in 7% acetic acid, 50% methanol and pure methanol. The membrane was blocked overnight at 4°C in TBS-Tween 0,2% (TBST) supplied with 5% milk. Primary antibody incubation was realized for 1h with 1:5000 (v/v) anti-GFP antibody (ab290, Abcam). The membrane was washed in TBST 5% milk, three times for 10min. Secondary antibody incubation was performed for 30min with 1:10000 (v/v) anti-rabbit IgG-peroxidase antibody (Sigma-

Aldrich). Again, the membrane was washed three times for 10min in TBST 5% milk, then three times for 10min in TBST. HRP substrates (Takara) and an iBrightTM CL750 Imaging System were used for immunodetection.

Bioinformatics

tRNA sequences and intron informations were retrieved from the PlantRNA 2.0 database (Cognat et al., 2022). tRNA structures were predicted using R2DT (Sweeney et al., 2021). EXTENSIN tandem repeats were determined with RADAR (Madeira et al., 2022). Bisulfite and ATAC-seq datasets were analysed as described in (Zhu et al., 2017; Hu et al., 2019), except that the reads mapping was conducted with a modified TAIR10 genome reference wherein the SYY cluster was replaced by one consensual SYY repeat sequence (REF1, **Supplemental Dataset 3**). Bisulfite files of roots: SRR578936, SRR578937, SRR578926, SRR578927. Bisulfite files of tissues: SRR3311817-SRR3311822 and SRR3311824-SRR3311825. ATAC-seq files of inflorescences: SRR12362020, SRR12362021, SRR12362026, SRR12362027.

Microscopy and image analysis

WISH-TSA images were acquired with a KERN OPTICS OZL 464 stereo microscope supplied with a tablet Cam ODC 241 (KERN). FISH results were screenshot with a LSM700 confocal microscope (Zeiss). The accumulation of EXT19-GFP-NLS was captured using a LSM880 confocal microscope (Zeiss), and ZEN black v2.3 software. The EXT19-GFP-NLS accumulation in Col-0 and *syy-1* backgrounds was analysed with an Olympus IX83 microscope, supplied with an Olympus XM10 camera and the CellSens Dimension v1.11 software (Olympus). GFP fluorescence was quantified in tips using ImageJ. Images were first converted in 8bits, and the “threshold” function was used with following parameters: 40, 255, default, B&W, and dark background. Integrated density was then measured in a circular area of 350x350 pixels.

Miscellaneous

Informations related to oligodeoxyribonucleotides used in this work can be found in **Supplemental Table 1**. They were either synthetized by Eurofins or Sigma-Aldrich.

ACKNOWLEDGMENTS

We thank the computing supports by the High Performance and Cloud Computing Group at the Zentrum für Datenverarbeitung of the University of Tübingen, the Baden-Württemberg state through bwHPC, and the German Research Foundation through grant no. INST 37/935-1 FUGG. The work was supported by the European Research Council under the European Union's Horizon 2020 research and innovation programme (grant no. 757600), and intramural funding from the University of Hohenheim. Moreover, this investigation was supported by founding from the National Natural Science Foundation of China (grant no. 32388201), the Strategic Priority Research Program of the Chinese Academy of Sciences (grant no. XDB27030101), and New Cornerstone Science Foundation through XPLORER PRIZE. We acknowledge Dr. Kerstin Feistel (Department of Zoology, University of Hohenheim), for her assistance in image acquisition with the LSM700 microscope, and Dr. Jean Molinier (Institut de biologie moléculaire des plantes, University of Strasbourg) for having provided the *rdd* mutant. The Max Planck Institute for Biology Tübingen is acknowledged for having shared some CRISPR/Cas9 vectors.

AUTHORS CONTRIBUTION

Conceptualization: G.H., P.K., C.L.
Data acquisition and analysis: G.H., P.K., C.L., N.S., N.W., L.W., Y.X.M., E.C.K.
Manuscript writing: G.H.
Manuscript editing: All authors participated equally.
Funding acquisition: C.L., J.W.W.

REFERENCES

Andras, S.C., Power, J.B., Cocking, E.C., and Davey, M.R. (2001). Strategies for signal amplification in nucleic acid detection. Mol. Biotechnol. **19**: 29–44.

Beier, D., Stange, N., Gross, H.J., and Beier, H. (1991). Nuclear tRNATyr genes are highly amplified at a single chromosomal site in the genome of Arabidopsis thaliana. MGG Mol. Gen. Genet. **225**: 72–80.

Benoit, M., Layat, E., Tourmente, S., and Probst, A.V. (2013). Heterochromatin dynamics during developmental transitions in Arabidopsis - a focus on ribosomal DNA loci. Gene **526**: 39–45.

Berg, M.D. and Brandl, C.J. (2021). Transfer RNAs: diversity in form and function. RNA Biol. **18**: 316–339.

Berg, P., Bergmann, F.H., Ofengand, E.J., and Dieckmann, M. (1961). The enzymic synthesis of amino acyl derivatives of ribonucleic acid. I. The mechanism of leucyl-, valyl-, isoleucyl-, and methionyl ribonucleic acid formation. J. Biol. Chem. **236**: 1726–1734.

Besser, D., Götz, F., Schulze-Forster, K., Wagner, H., Kröger, H., and Simon, D. (1990). DNA methylation inhibits transcription by RNA polymerase III of a tRNA gene, but not of a 5S rRNA gene. FEBS Lett.

Böhmdorfer, G., Sethuraman, S., Rowley, M.J., Krzyszton, M., Rothi, M.H., Bouzit, L., and Wierzbicki, A.T. (2016). Long non-coding RNA produced by RNA polymerase V determines boundaries of heterochromatin. Elife **5**: e19092.

Bourguet, P., Picard, C.L., Yelagandula, R., Pélissier, T., Lorković, Z.J., Feng, S., Pouch-Pélissier, M.N., Schmücker, A., Jacobsen, S.E., Berger, F., and Mathieu, O. (2021). The histone variant H2A.W and linker histone H1 co-regulate heterochromatin accessibility and DNA methylation. Nat. Commun. **12**: 2683.

Canella, D., Praz, V., Reina, J.H., Cousin, P., and Hernandez, N. (2010). Defining the RNA polymerase III transcriptome: Genome-wide localization of the RNA polymerase III transcription machinery in human cells. Genome Res. **20**: 710–721.

Castilleux, R., Plancot, B., Ropitaux, M., Carreras, A., Leprince, J., Boulogne, I., Follet-Gueye, M.L., Popper, Z.A., Driouich, A., and Vicré, M. (2018). Cell wall extensins in root–microbe interactions and root secretions. J. Exp. Bot. **69**: 4235–4247.

Chan, P.P. and Lowe, T.M. (2016). GtRNAdb 2.0: an expanded database of transfer RNA genes identified in complete and draft genomes. Nucleic Acids Res. **44**: D184–D189.

Chang, S., Puryear, J., and Cairney, J. (1993). A simple and efficient method for isolating RNA from pine trees. Plant Mol. Biol. Report. **11**: 113–116.

Chevallier, A. and Garel, J.P. (1982). Differential synthesis rates of tRNA species in the silk gland of Bombyx mori are required to promote tRNA adaptation to silk messages. Eur. J. Biochem. **124**: 477–482.

Cloix, C., Tutois, S., Yukawa, Y., Mathieu, O., Cuvillier, C., Espagnol, M.C., Picard, G., and Tourmente, S. (2002). Analysis of the 5S RNA pool in Arabidopsis thaliana: RNAs are heterogeneous and only two of the genomic 5S loci produce mature 5S RNA. Genome Res. **12**: 132–144.

Cognat, V., Pawlak, G., Pflieger, D., and Drouard, L. (2022). PlantRNA 2.0: an updated database dedicated to tRNAs of photosynthetic eukaryotes. Plant J. **112**: 1112–1119.

Dolan, L., Janmaat, K., Willemsen, V., Linstead, P., Poethig, S., Roberts, K., and Scheres, B. (1993). Cellular organisation of the Arabidopsis thaliana root. Development **119**: 71–84.

Driouich, A., Gaudry, A., Pawlak, B., and Moore, J.P. (2021). Root cap-derived cells and mucilage: a protective network at the root tip. Protoplasma **258**: 1179–1185.

Feng, D. et al. (2022). Chromatin accessibility illuminates single-cell regulatory dynamics of rice root tips. BMC Biol. **20**: 274.

Fultz, D., McKinlay, A., Enganti, R., and Pikaard, C.S. (2023). Sequence and epigenetic landscapes of active and silenced nucleolus organizers in Arabidopsis. bioRxiv.

Gage, L.P. and Manning, R.F. (1980). Internal structure of the silk fibroin gene of Bombyx mori. I The fibroin gene consists of a homogeneous alternating array of repetitious crystalline and amorphous coding sequences. J. Biol. Chem. **255**: 9444–9450.

Garel, J.P., Fournier, A., and Daillie, J. (1973). Functional and modulatory adaptation of tRNA in the silk gland of bombyx mori L. to fibroin biosynthesis. Hoppe Seylers Z

Physiol Chem. **354**: 600.

Giegé, R. and Eriani, G. (2023). The tRNA identity landscape for aminoacylation and beyond. Nucleic Acids Res. **51**: 1528–1570.

Gogakos, T., Brown, M., Garzia, A., Meyer, C., Hafner, M., and Tuschl, T. (2017). Characterizing expression and processing of precursor and mature human tRNAs by hydro-tRNAseq and PAR-CLIP. Cell Rep. **20**: 1463–1475.

Goodenbour, J.M. and Pan, T. (2006). Diversity of tRNA genes in eukaryotes. Nucleic Acids Res. **34**: 6137–6146.

Green, G.A. and Weil, J.. H. (1989). Evolution of a plant nuclear tRNA Pro gene cluster. Plant Mol. Biol. **13**: 727–730.

Hellens, R.P., Edwards, E.A., Leyland, N.R., Bean, S., and Mullineaux, P.M. (2000). pGreen: a versatile and flexible binary Ti vector for Agrobacterium-mediated plant transformation. Plant Mol. Biol. **42**: 819–832.

Hijazi, M., Velasquez, S.M., Jamet, E., Estevez, J.M., and Albenne, C. (2014). An update on post-translational modifications of hydroxyproline-rich glycoproteins: Toward a model highlighting their contribution to plant cell wall architecture. Front. Plant Sci.: 5:395.

Hoagland, M.B., Stephenson, M.L., Scott, J.F., Hecht, L.I., and Zamecnik, P.C. (1958). A soluble ribonucleic acid intermediate in protein synthesis. J. Biol. Chem. **231**: 241–257.

Holley, R.W., Apgar, J., Everett, G.A., Madison, J.T., Marquisee, M., Merrill, S.H., Penswick, J.R., and Zamir, A. (1965). Structure of a ribonucleic acid. Science **147**: 1462–1465.

Hu, B., Wang, N., Bi, X., Karaaslan, E.S., Weber, A.L., Zhu, W., Berendzen, K.W., and Liu, C. (2019). Plant lamin-like proteins mediate chromatin tethering at the nuclear periphery. Genome Biol. **20**: 87.

Hughes, L.A., Rudler, D.L., Siira, S.J., McCubbin, T., Raven, S.A., Browne, J.M., Ermer, J.A., Rientjes, J., Rodger, J., Marcellin, E., Rackham, O., and Filipovska, A. (2023). Copy number variation in tRNA isodecoder genes impairs mammalian development and balanced translation. Nat. Commun. **14**: 2210.

Hummel, G., Berr, A., Graindorge, S., Cognat, V., Ubrig, E., Pflieger, D., Molinier, J.,

and Drouard, L. (2020). Epigenetic silencing of clustered tRNA genes in Arabidopsis. Nucleic Acids Res. **48**: 10297–10312.

Hummel, G. and Liu, C. (2022). Organization and epigenomic control of RNA polymerase III-transcribed genes in plants. Curr. Opin. Plant Biol. **67**: 102199.

Hummel, G., Warren, J., and Drouard, L. (2019). The multi-faceted regulation of nuclear tRNA gene transcription. IUBMB Life **71**: 1099–1108.

Johnson, K.C.M., Yu, Y., Gao, L., Eng, R.C., Wasteneys, G.O., Chen, X., and Li, X. (2016). A partial loss-of-function mutation in an Arabidopsis RNA polymerase III subunit leads to pleiotropic defects. J. Exp. Bot. **67**: 2219–2230.

Kawakatsu, T., Stuart, T., Valdes, M., Breakfield, N., Schmitz, R.J., Nery, J.R., Urich, M.A., Han, X., Lister, R., Benfey, P.N., and Ecker, J.R. (2016). Unique cell-type specific patterns of DNA methylation in the root meristem. Nat. Plants **2**: 16058.

Law, J.A. and Jacobsen, S.E. (2010). Establishing, maintaining and modifying DNA methylation patterns in plants and animals. Nat. Rev. Genet. **11**: 204–220.

Liu, K. and Sun, Q. (2021). Intragenic tRNA-promoted R-loops orchestrate transcription interference for plant oxidative stress responses. Plant Cell **33**: 3574–3591.

Ma, X., Liu, C., Kong, X., Liu, J., Zhang, S., Liang, S., Luan, W., and Cao, X. (2021). Extensive profiling of the expressions of tRNAs and tRNA-derived fragments (tRFs) reveals the complexities of tRNA and tRF populations in plants. Sci. China Life Sci. **64**: 495–511.

Madeira, F., Pearce, M., Tivey, A.R.N., Basutkar, P., Lee, J., Edbali, O., Madhusoodanan, N., Kolesnikov, A., and Lopez, R. (2022). Search and sequence analysis tools services from EMBL-EBI in 2022. Nucleic Acids Res. **50**: W276–W279.

Majima, R., Kawakami, M., and Shimura, K. (1975). The biosynthesis of transfer RNA in insects. I. Increase of amino acid acceptor activity of specific tRNA's utilized for silk protein biosynthesis in the silk gland of Bombyx mori. J. Biochem. **78**: 391–400.

Manning, R.F. and Gage, L.P. (1978). Physical map of the Bombyx mori DNA containing the gene for silk fibroin. J. Biol. Chem. **253**: 2044–2052.

Mathieu, O., Jasencakova, Z., Vaillant, I., Gendrel, A.V., Colot, V., Schubert, I., and

Tourmente, S. (2003). Changes in 5S rDNA chromatin organization and transcription during heterochromatin establishment in Arabidopsis. Plant Cell **15**: 2929–2939.

Mathieu, O., Yukawa, Y., Sugiura, M., Picard, G., and Tourmente, S. (2002). 5S rRNA genes expression is not inhibited by DNA methylation in Arabidopsis. Plant J. **29**: 313–323.

Michaud, M., Cognat, V., Duchêne, A.M., and Maréchal-Drouard, L. (2011). A global picture of tRNA genes in plant genomes. Plant J. **66**: 80–93.

Michiels, A., Van den Ende, W., Tucker, M., Van Riet, L., and Van Laere, A. (2003). Extraction of high-quality genomic DNA from latex-containing plants. Anal. Biochem. **315**: 85–89.

Montgomery, S.A., Hisanaga, T., Wang, N., Axelsson, E., Akimcheva, S., Sramek, M., Liu, C., and Berger, F. (2022). Polycomb-mediated repression of paternal chromosomes maintains haploid dosage in diploid embryos of Marchantia. Elife **11**: e79258.

Moqtaderi, Z., Wang, J., Raha, D., White, R.J., Snyder, M., Weng, Z., and Struhl, K. (2010). Genomic binding profiles of functionally distinct RNA polymerase III transcription complexes in human cells. Nat. Struct. Mol. Biol.

Moussu, S. and Ingram, G. (2023). The EXTENSIN enigma. Cell Surf. **9**: 100094.

Nirenberg, M.W., Leder, P., Bernfield, M., Brimacombe, R., Trupin, J., Rottman, F., and O'Neal, C. (1965). RNA codewords and protein synthesis, VII. On the general nature of the RNA code. Proc. Natl. Acad. Sci. U. S. A. **53**: 1161–1168.

Norris, S.R., Meyer, S.E., and Callis, J. (1993). The intron of Arabidopsis thaliana polyubiquitin genes is conserved in location and is a quantitative determinant of chimeric gene expression. Plant Mol. Biol. **21**: 895–906.

Oler, A.J., Alla, R.K., Roberts, D.N., Wong, A., Hollenhorst, P.C., Chandler, K.J., Cassiday, P.A., Nelson, C.A., Hagedorn, C.H., Graves, B.J., and Cairns, B.R. (2010). Human RNA polymerase III transcriptomes and relationships to Pol II promoter chromatin and enhancer-binding factors. Nat. Struct. Mol. Biol. **17**: 620–628.

Osakabe, A., Jamge, B., Axelsson, E., Montgomery, S.A., Akimcheva, S., Kuehn,

A.L., Pisupati, R., Lorković, Z.J., Yelagandula, R., Kakutani, T., and Berger, F. (2021). The chromatin remodeler DDM1 prevents transposon mobility through deposition of histone variant H2A.W. Nat. Cell Biol. **23**: 391–400.

Osakabe, A., Takizawa, Y., Horikoshi, N., Hatazawa, S., Negishi, L., Berger, F., Kakutani, T., and Kurumizaka, H. (2023). Molecular and structural basis of the heterochromatin-specific chromatin remodeling activity by Arabidopsis DDM1. bioRxiv.

Parthasarthy, A. and Gopinathan, K.P. (2005). Modulation of differential transcription of tRNA genes through chromatin organization. Biochem. J. **391**: 371–381.

Penterman, J., Zilberman, D., Huh, J.H., Ballinger, T., Henikoff, S., and Fischer, R.. (2007). DNA demethylation in the Arabidopsis genome. Proc. Natl. Acad. Sci. U. S. A. **104**: 6752–6757.

Phizicky, E.M. and Hopper, A.K. (2023). The life and times of a tRNA. RNA **29**: 898–957.

Probst, A.V. (2022). Deposition and eviction of histone variants define functional chromatin states in plants. Curr. Opin. Plant Biol. **69**: 102266.

Probst, A.V., Desvoyes, B., and Gutierrez, C. (2020). Similar yet critically different: the distribution, dynamics and function of histone variants. J. Exp. Bot. **71**: 5191–5204.

Rabanal, F.A., Gräff, M., Lanz, C., Fritschi, K., Llaca, V., Lang, M., Carbonell-Bejerano, P., Henderson, I., and Weigel, D. (2022). Pushing the limits of HiFi assemblies reveals centromere diversity between two Arabidopsis thaliana genomes. Nucleic Acids Res. **50**: 12309–12327.

Rifkind, R.A., Marks, P.A., Bank, A., Terada, M., Maniatis, G.M., Reuben, R., and Fibach, E. (1976). Erythroid differentiation and the cell cycle: some implications from murine foetal and erythroleukemic cells. Ann Immunol **127**: 887–893.

Roeder, R.G. (2019). 50+ years of eukaryotic transcription: an expanding universe of factors and mechanisms. Nat. Struct. Mol. Biol. **26**: 783–791.

Rosa, S., Ntoukakis, V., Ohmido, N., Pendle, A., Abranches, R., and Shaw, P. (2014). Cell differentiation and development in Arabidopsis are associated with changes in histone dynamics at the single-cell level. Plant Cell **26**: 4821–4833.

Santamaría-Gómez, J., Rubio, M.Á., López-Igual, R., Romero-Losada, A.B.,

Delgado-Chaves, F.M., Bru-Martínez, R., Romero-Campero, F.J., Herrero, A., Ibba, M., Ochoa de Alda, J.A.G., and Luque, I. (2021). Role of a cryptic tRNA gene operon in survival under translational stress. Nucleic Acids Res. **49**: 8757–8776.

Santos, A.P., Gaudin, V., Mozgová, I., Pontvianne, F., Schubert, D., Tek, A.L., Dvořáčková, M., Liu, C., Fransz, P., Rosa, S., and Farrona, S. (2020). Tidying-up the plant nuclear space: Domains, functions, and dynamics. J. Exp. Bot. **71**: 5160–5178.

Santos, F.B. and Del-Bem, L.E. (2022). The evolution of tRNA copy number and repertoire in cellular life. Genes (Basel). **14**: 27.

Showalter, A.M. (1993). Structure and function of plant cell wall proteins. Plant Cell **5**: 9–23.

Showalter, A.M., Keppler, B., Lichtenberg, J., Gu, D., and Welch, L.R. (2010). A bioinformatics approach to the identification, classification, and analysis of hydroxyproline-rich glycoproteins. Plant Physiol. **153**: 485–513.

Shukla, A. and Bhargava, P. (2018). Regulation of tRNA gene transcription by the chromatin structure and nucleosome dynamics. Biochim. Biophys. Acta - Gene Regul. Mech. **1861**: 295–309.

Siddiqui, M.A. and Chen, G.S. (1975). Biosynthesis of tRNA in the posterior silk gland of Bombyx mori. Brookhaven Symp Biol. **26**: 154–164.

Simon, L. and Probst, A.V. (2023). Maintenance and dynamic reprogramming of chromatin organization during development. Plant J.

Sizer, R.E., Chahid, N., Butterfield, S.P., Donze, D., Bryant, N.J., and White, R.J. (2022). TFIIIC-based chromatin insulators through eukaryotic evolution. Gene **835**: 146533.

Stutzman, A.V., Liang, A.S., Beilinson, V., and Ikegami, K. (2020). Transcription-independent TFIIIC-bound sites cluster near heterochromatin boundaries within lamina-associated domains in C. elegans. Epigenetics and Chromatin **13**: 1.

Sun, C.W. and Callis, J. (1997). Independent modulation of Arabidopsis thaliana polyubiquitin mRNAs in different organs and in response to environmental changes. Plant J. **11**: 1017–1027.

Sweeney, B.A. et al. (2021). R2DT is a framework for predicting and visualising RNA secondary structure using templates. Nat. Commun. **12**: 3494.

Theologis, A. et al. (2000). Sequence and analysis of chromosome 1 of the plant Arabidopsis thaliana. Nature **408**: 816–820.

Thornlow, B.P., Hough, J., Roger, J.M., Gong, H., Lowe, T.M., and Corbett-Detig, R.B. (2018). Transfer RNA genes experience exceptionally elevated mutation rates. Proc. Natl. Acad. Sci. U. S. A. **115**: 8996–9001.

Torres, A.G. (2019). Enjoy the silence: nearly half of human tRNA genes are silent. Bioinform. Biol. Insights **13**: 1–3.

Torres, A.G., Reina, O., Attolini, C.S.O., and de Pouplana, L.R. (2019). Differential expression of human tRNA genes drives the abundance of tRNA-derived fragments. Proc. Natl. Acad. Sci. U. S. A. **116**: 8451–8456.

Underwood, D.C., Knickerbocker, H., Gardner, G., Condliffe, D.P., and Sprague, K.U. (1988). Silk gland-specific tRNA(Ala) genes are tightly clustered in the silkworm genome. Mol. Cell. Biol. **8**: 5504–5512.

Varshney, D., Vavrova-Anderson, J., Oler, A.J., Cowling, V.H., Cairns, B.R., and White, R.J. (2015). SINE transcription by RNA polymerase III is suppressed by histone methylation but not by DNA methylation. Nat. Commun. **6**: 6569.

Vongs, A., Kakutani, T., Martienssen, R.A., and Richards, E.J. (1993). Arabidopsis thaliana DNA methylation mutants. Science (80-.). **260**: 1926–1928.

Walbot, V. (1972). Rate of RNA synthesis and tRNA end-labeling during early development of Phaseolus. Planta **108**: 161–171.

Wang, N., Karaaslan, E.S., Faiss, N., Berendzen, K.W., and Liu, C. (2021). Characterization of a plant nuclear matrix constituent protein in liverwort. Front. Plant Sci. **12**: 670306.

Wlodzimierz, P. et al. (2023). Cycles of satellite and transposon evolution in Arabidopsis centromeres. Nature **618**: 557–565.

Wójcik, A.M., Mosiolek, M., Karcz, J., Nodine, M.D., and Gaj, M.D. (2018). Whole mount in situ localization of miRNAs and mRNAs during somatic embryogenesis in Arabidopsis. Front. Plant Sci. **9**: 1277.

Wu, R., Lucke, M., Jang, Y.-T., Zhu, W., Symeonidi, E., Wang, C., Fitz, J., Xi, W.,

Schwab, R., and Weigel, D. (2018). An efficient CRISPR vector toolbox for engineering large deletions in Arabidopsis thaliana. Plant Methods **14**: 65.

Yague-Sanz, C., Migeot, V., Larochelle, M., Bachand, F., Wéry, M., Morillon, A., and Hermand, A. (2023). Chromatin remodeling by Pol II primes efficient Pol III transcription. Nat. Commun. **14**: 3587.

Yukawa, Y., Sugita, M., Choisne, N., Small, I., and Sugiura, M. (2000). The TATA motif, the CAA motif and the poly(T) transcription termination motif are all important for transcription re-initiation on plant tRNA genes. Plant J. **22**: 439–447.

Zemach, A., Kim, M.Y., Hsieh, P.H., Coleman-Derr, D., Eshed-Williams, L., Thao, K., Harmer, S.L., and Zilberman, D. (2013). The Arabidopsis nucleosome remodeler DDM1 allows DNA methyltransferases to access H1-containing heterochromatin. Cell **153**: 193–205.

Zhang, H., Lang, Z., and Zhu, J.K. (2018). Dynamics and function of DNA methylation in plants. Nat. Rev. Mol. Cell Biol. **19**: 489–506.

Zhang, T.Q., Chen, Y., Liu, Y., Lin, W.H., and Wang, J.W. (2021). Single-cell transcriptome atlas and chromatin accessibility landscape reveal differentiation trajectories in the rice root. Nat. Commun. **12**: 2053.

Zhang, Z., Mao, Y., Ha, S., Liu, W., Botella, J.R., and Zhu, J.K. (2016). A multiplex CRISPR/Cas9 platform for fast and efficient editing of multiple genes in Arabidopsis. Plant Cell Rep. **35**: 1519–1533.

Zhong, Z., Feng, S., Duttke, S.H., Potok, M.E., Zhang, Y., Gallego-Bartolomé, J., Liu, W., and Jacobsen, S.E. (2021). DNA methylation-linked chromatin accessibility affects genomic architecture in Arabidopsis. Proc. Natl. Acad. Sci. U. S. A. **118**: e2023347118.

Zhu, W., Hu, B., Becker, C., Doğan, E.S., Berendzen, K.W., Weigel, D., and Liu, C. (2017). Altered chromatin compaction and histone methylation drive non-additive gene expression in an interspecific Arabidopsis hybrid. Genome Biol. **18**: 157.

FIGURE LEGENDS

Figure 1, Expression pattern of the SYY cluster during vegetative development

A, Representative thumbnails of 0, 1, 2, 3, 4 and 14DAS germination timepoints. **B,** Segmentation of a 7DAS plant. T: total, S: shoot, R: root, LR: lower root. S1, S2 and S3 refer to elongation, transition, and mitosis + tip. **C,** D/C-tRNAs^{Tyr} and D-tRNAs^{Ala} accumulation during germination. Two equal exposures (E1, 2) are presented for D/C-tRNAs^{Tyr}. Histograms correspond to the quantification of C-tRNAs^{Tyr} in three independent replicates. **D,** C-tRNAs^{Tyr} and D-tRNAs^{Ala} accumulation in organs, epigenetic and RNAP mutants.

Figure 2, Generation and transformation of deletion alleles with tRNA genes

A, Screening procedure for lines lacking the SYY cluster. Dual ("GH", in black) and multiplexed ("LW", in grey) gRNAs (scissors) used in A/B regions are detailed in **B**, with proximal genomic entities. DZ, deletion zone. **C and D,** PCR profile of homozygous lines. Black arrows point ladder (L) sizes the closest from amplicons, while white ones indicate closest sizes of putative amplicons according to TAIR10 genome. **E,** Sequence of *syy-1* and *syy-2* alleles. Few nucleotides up and downstream (green and yellow regions in **A** of the DNA junction (GC/TC di-nucleotides) are shown. **F,** D/C-tRNAs^{Tyr} and D-tRNAs^{Ala} steady-state levels in Col-0, *syy-1* and *syy-2* 7DAS roots. **G,** Stable agro-transformation of *syy-1* background with transgenic tRNA genes. In Ing-Y construct, bold sequence corresponds to the major C-tRNA^{Tyr}. Brackets delimitate intron. Within up and downstream regions (in grey), the A/T-rich region and poly-T stretch are demarked with arrows. TATA-like and CAA *cis*-motifs are highlighted in purple. **H,** C-tRNAs^{Tyr} and D-tRNAs^{Ala} steady-state levels in Col-0, *syy-1*, *syy-1* Ing-Y (three independent lines), and *syy-1* 1xSYY (two independent lines) 7DAS roots. 1+2 = 4543bps (*syy-1* screen) or 5228bps (*syy-2* screen). 3+2 = 547bps (*syy-1* screen) or 1875bps (*syy-2* screen). α+β = 408bps. γ+δ = 564bps. ε+ζ = 212bps.

Figure 3, Expression pattern of the SYY cluster within root tissues

A, WISH-TSA detection of C-tRNAs^{Tyr} within 4DAS Col-0 and *syy-1* rootlets. Grey-outlined arrows point zones of differential staining between genotypes. Black arrows proportionally subdivide S1, S2 and S3 segments. **B,** Enlargements of 4DAS Col-0 and *syy-1* tips. The four external columella (RCC1-4) and lateral root cap (LRC) cells with a strong C-tRNAs^{Tyr} accumulation are titled with grey-dotted lines. Three representatives are depicted.

Figure 4, Methylation landscape of natural and transgenic SYY repeats in roots

A, Chop-PCR amplification of Val, Y1 and Y2 loci with Col-0 root S1, S2 and S3 genomic DNA. **B,** Relative chop-PCR product amounts by gene, digested cytosine context and root segment. Mock quantification value is arbitrarily set to 1. Histograms represent the mean of three independent biological replicates, and bars the standard deviation. **C,** Chop-PCR amplification of Val and Y2 loci with Col-0 and *syy-1* 1xSYY total root genomic DNAs. Two independent *syy-1* 1xSYY lines are presented. **D,** Methylation levels at S, Y1 and Y2 loci in whole tip and columella genomic DNA. Bars represent the ratio of methylated cytosines in 20bps bins.

Figure 5, Mimicry of a high Ser, Tyr, and Pro translational demand *in vivo*

A, Identification of proteins co-enriched in Ser, Tyr, and Pro encoded within the *A. thaliana* Col-0 genome. Names of the top five candidates are flagged. **B,** Reporter construct (RC) design used to monitor high Ser, Tyr, and Pro translation. In the EXT19 coding sequence, initiator Met is in green, Ser and Tyr residues are in red whereas Pro ones in blue. Putative secretion motif is highlighted in yellow. **C,** A 14DAS Col-0 RC root. S1, S2 and S3 sections are demarcated with dotted lines. The arrow marks out the major EXT19-GFP-NLS accumulation site in S3. **D,** Cellular resolution of a 2DAS Col-0 RC tip. Full lines designate the cell layers (L1 and L2) hosting a high EXT19-GFP-NLS accumulation. Dotted lines precise L1 RCC and LRC cells.

Figure 6, Translational capacity of Col-0 and *syy-1* root cells

A, Analysis of EXT19-GFP-NLS accumulation in Col-0 and *syy-1* tips by epifluorescence. Three independent lines (L) are shown by genotype. For each, three representatives are depicted. **B,** Distribution of GFP fluorescence intensity by genotype and line. 50 individuals (n) were analysed by line. A one-way ANOVA test disclosed a significant difference in GFP fluorescence between Col-0 and *syy-1* populations ($P < 2x10^{-16}$, ***). Thumbnails in A were selected based on a homogenous dispersal around medians plotted in B (*i.e.,* +/- 500000). **C,** Analysis of EXT19-GFP-NLS accumulation in Col-0 and *syy-1* total roots by western blot. f.p.: fusion protein, n.b.: nonspecific bands, s.p.: short products.

Figure 1, Expression pattern of the SYY cluster during vegetative development

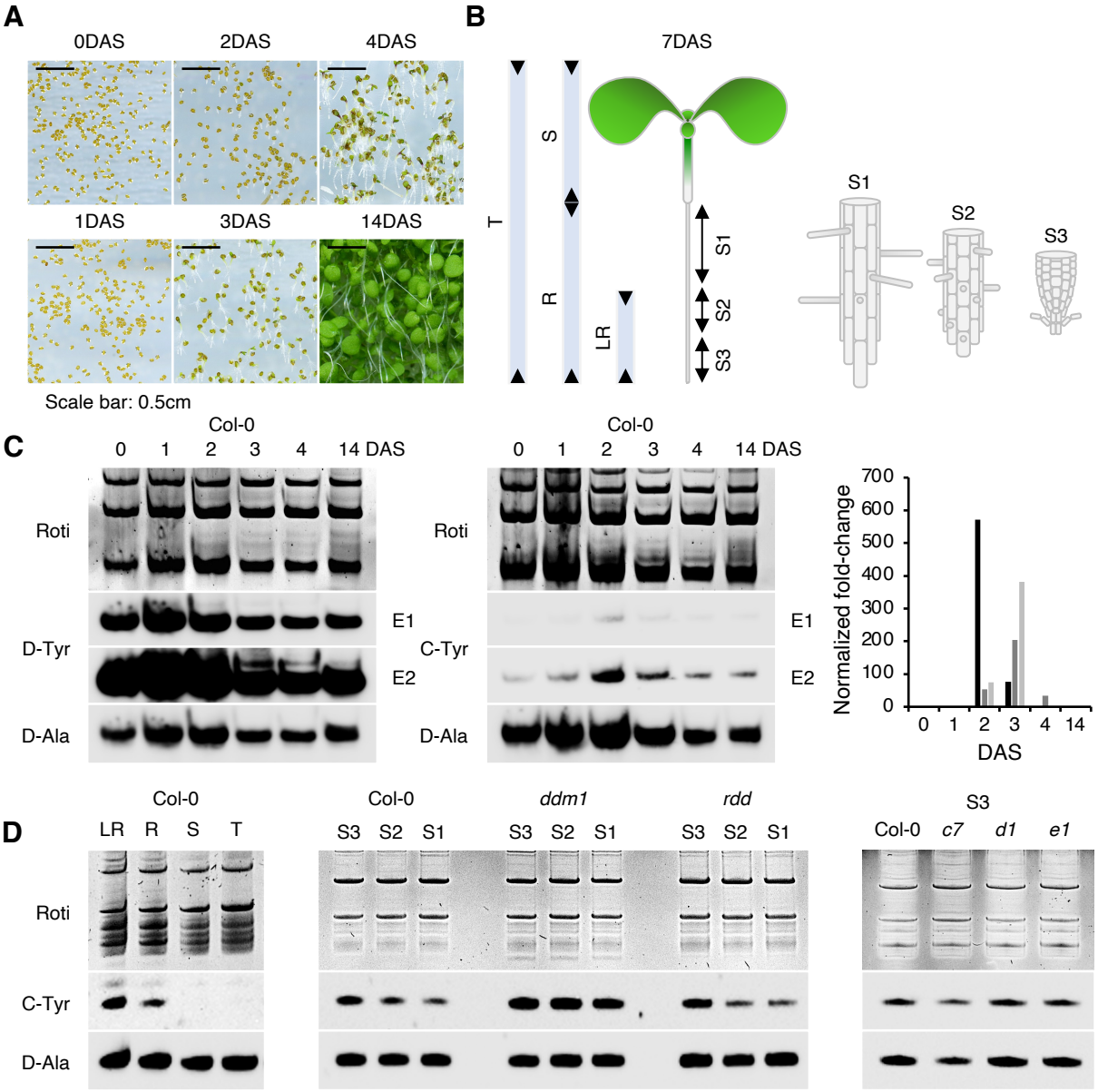

Figure 1, Expression pattern of the SYY cluster during vegetative development

A, Representative thumbnails of 0, 1, 2, 3, 4 and 14DAS germination timepoints. **B,** Segmentation of a 7DAS plant. T: total, S: shoot, R: root, LR: lower root. S1, S2 and S3 refer to elongation, transition, and mitosis + tip. **C,** D/C-tRNAs^{Tyr} and D-tRNAs^{Ala} accumulation during germination. Two equal exposures (E1, 2) are presented for D/C-tRNAs^{Tyr}. Righten histograms correspond to the quantification of C-tRNAs^{Tyr} in three independent replicates. **D,** C-tRNAs^{Tyr} and D-tRNAs^{Ala} accumulation in organs, epigenetic and RNAP mutants.

Figure 2, Generation and transformation of deletion alleles with tRNA genes

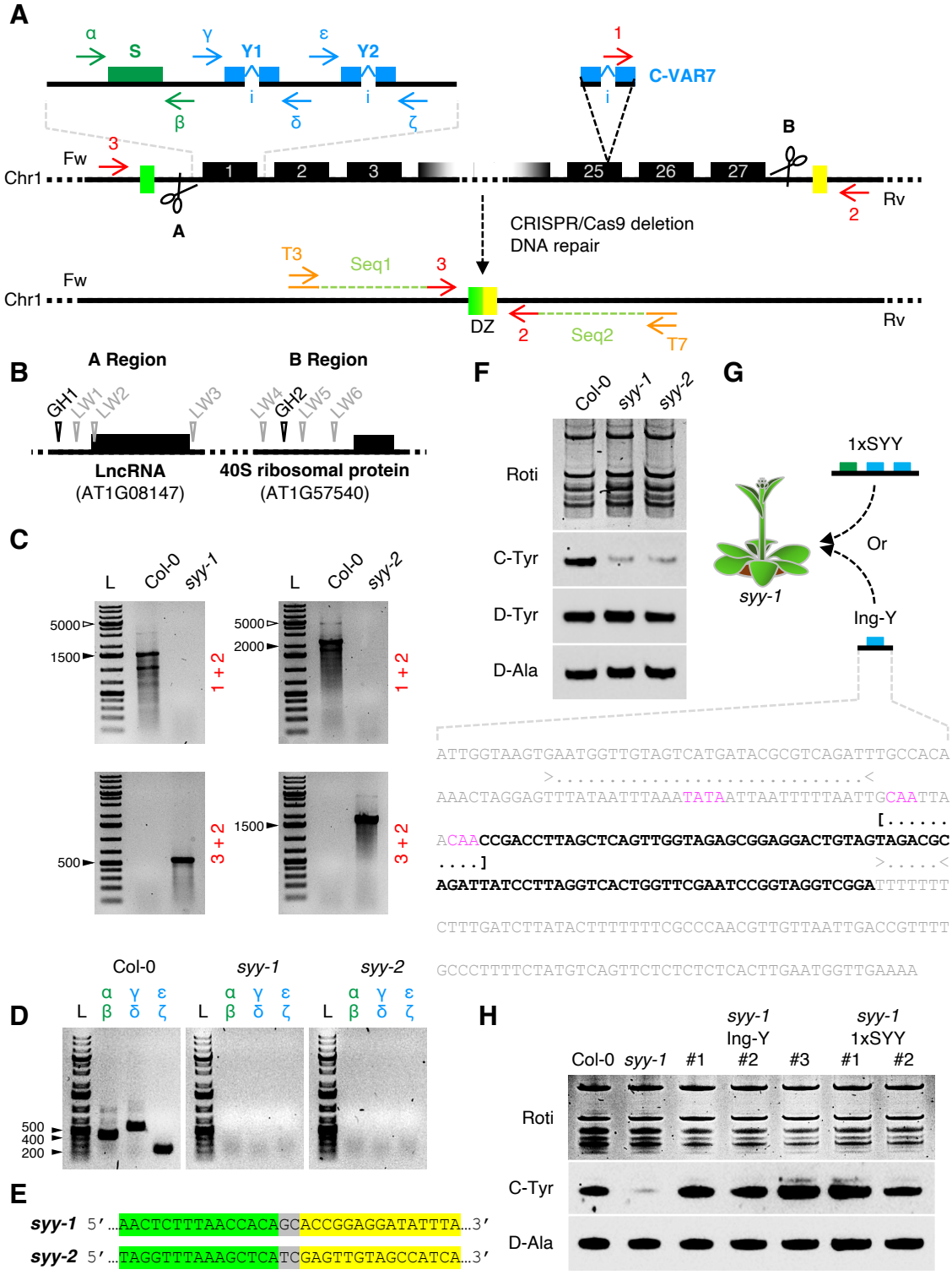

Figure 2, Generation and transformation of deletion alleles with tRNA genes

A, Screening procedure for lines lacking the SYY cluster. Dual ("GH", in black) and multiplexed ("LW", in grey) gRNAs (scissors) used in A/B regions are detailed in **B**, with proximal genomic entities. DZ, deletion zone. **C and D,** PCR profile of homozygous lines. Black arrows point ladder (L) sizes the closest from amplicons, while white ones indicate closest sizes of putative amplicons according to TAIR10 genome. **E,** Sequence of *syy-1* and *syy-2* alleles. Few nucleotides up and downstream (green and yellow regions in **A** of the DNA junction (GC/TC di-nucleotides) are shown. **F,** D/C-tRNAs^{Tyr} and D-tRNAs^{Ala} steady-state levels in Col-0, *syy-1* and *syy-2* 7DAS roots. **G,** Stable agro-transformation of *syy-1* background with transgenic tRNA genes. In Ing-Y construct, bold sequence corresponds to the major C-tRNA^{Tyr}. Brackets delimitate intron. Within up and downstream regions (in grey), the A/T-rich region and poly-T stretch are demarked with arrows. TATA-like and CAA *cis*-motifs are highlighted in purple. **H,** C-tRNAs^{Tyr} and D-tRNAs^{Ala} steady-state levels in Col-0, *syy-1*, *syy-1* Ing-Y (three independent lines), and *syy-1* 1xSYY (two independent lines) 7DAS roots. 1+2 = 4543bps (*syy-1* screen) or 5228bps (*syy-2* screen). 3+2 = 547bps (*syy-1* screen) or 1875bps (*syy-2* screen). α+β = 408bps. γ+δ = 564bps. ε+ζ = 212bps.

Figure 3, Expression pattern of the SYY cluster within root tissues

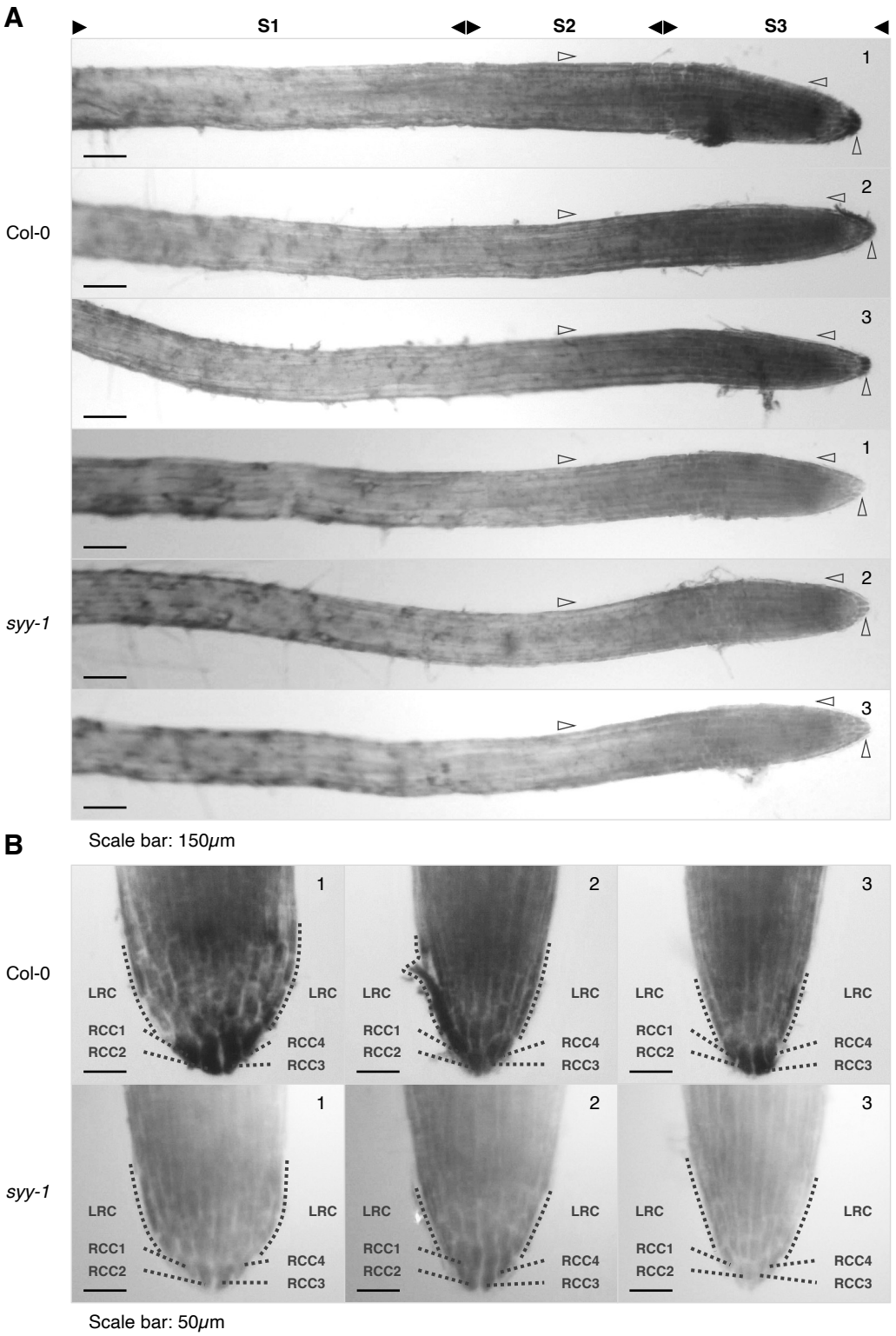

Figure 3, Expression pattern of the SYY cluster within root tissues

A, WISH-TSA detection of C-tRNAs^{Tyr} within 4DAS Col-0 and *syy-1* rootlets. Grey-outlined arrows point zones of differential staining between genotypes. Black arrows proportionally subdivide S1, S2 and S3 segments. **B,** Enlargements of 4DAS Col-0 and *syy-1* tips. The four external columella (RCC1-4) and lateral root cap (LRC) cells with a strong C-tRNAs^{Tyr} accumulation are titled with grey-dotted lines. Three representatives are depicted.

Figure 4, Methylation landscape of natural and transgenic SYY repeats in roots

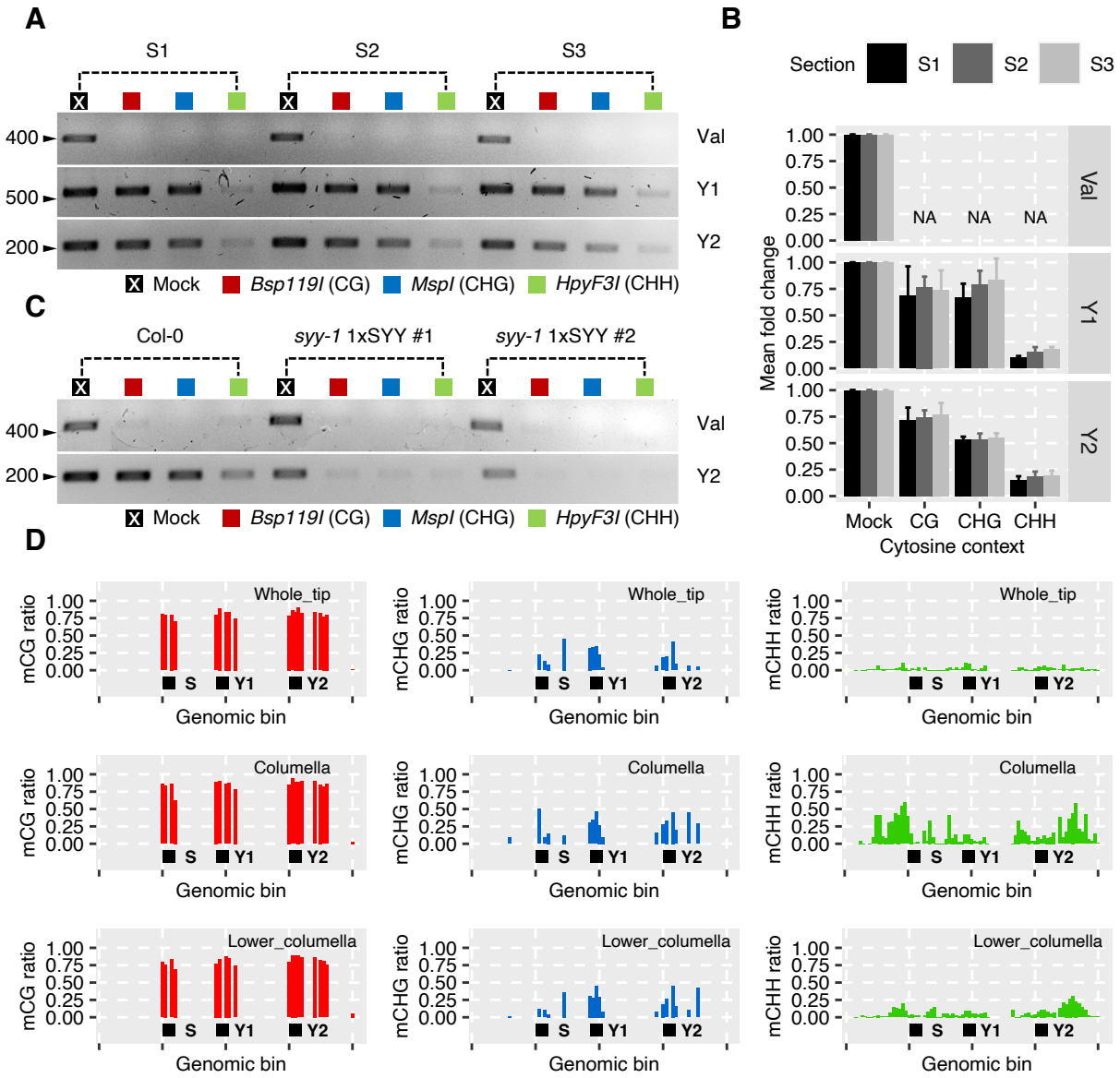

Figure 4, Methylation landscape of natural and transgenic SYY repeats in roots

A, Chop-PCR amplification of Val, Y1 and Y2 loci with Col-0 root S1, S2 and S3 genomic DNA. **B,** Relative chop-PCR product amounts by gene, digested cytosine context and root segment. Mock quantification value is arbitrarily set to 1. Histograms represent the mean of three independent biological replicates and bars the standard deviation. **C,** Chop-PCR amplification of Val and Y2 loci with Col-0 and *syy-1* 1xSYY total root genomic DNAs. Two independent *syy-1* 1xSYY lines are presented. **D,** Methylation levels at S, Y1 and Y2 loci in whole tip and columella genomic DNA. Bars represent the ratio of methylated cytosines in 20bps bins.

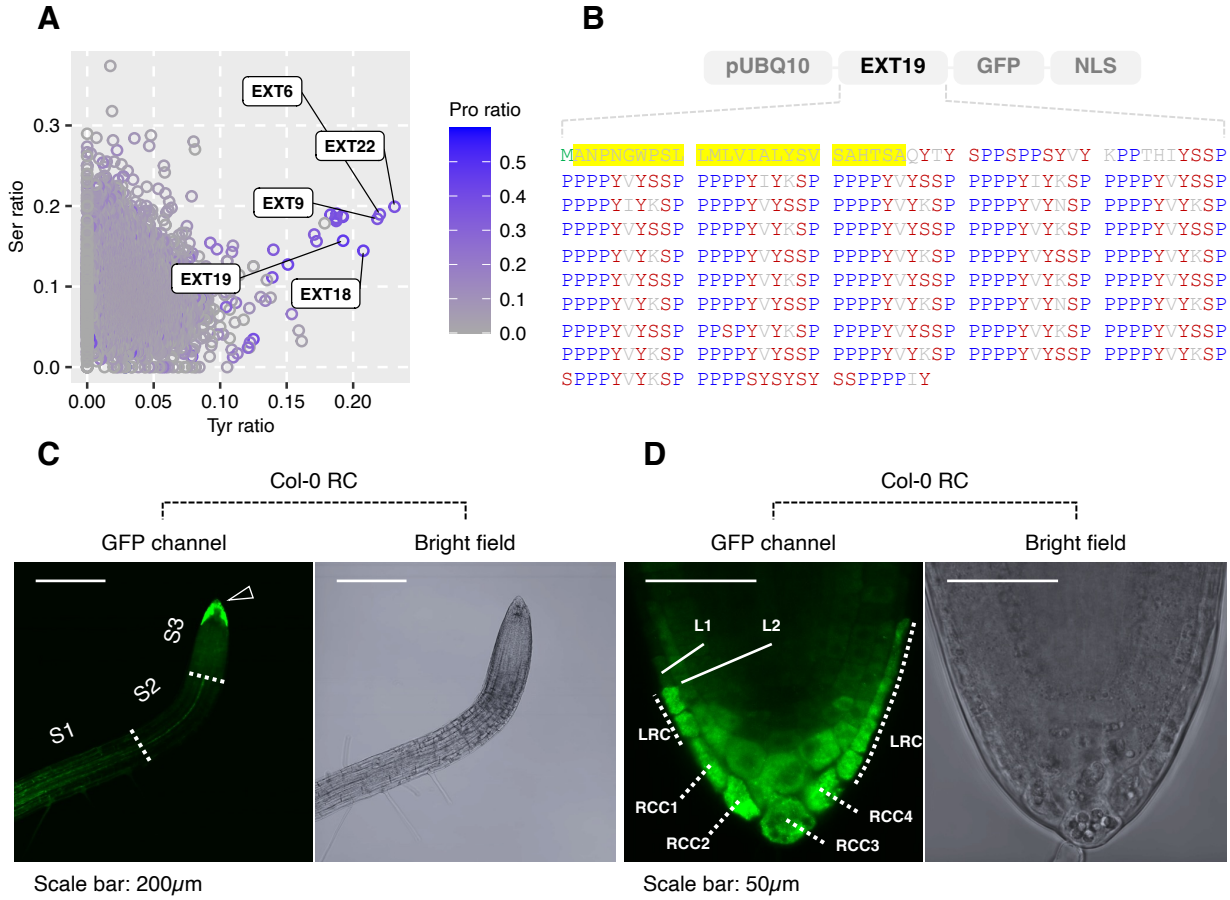

Figure 5, Mimicry of a high Ser, Tyr, and Pro translational demand *in vivo*

A, Identification of proteins co-enriched in Ser, Tyr, and Pro encoded within the *A. thaliana* Col-0 genome. Names of the top five candidates are flagged. **B,** Reporter construct (RC) design used to monitor high Ser, Tyr, and Pro translation. In the EXT19 coding sequence, initiator Met is in green, Ser and Tyr residues are in red whereas Pro ones in blue. Putative secretion motif is highlighted in yellow. **C,** A 14DAS Col-0 RC root. S1, S2 and S3 sections are demarcated with dotted lines. The arrow marks out the major EXT19-GFP-NLS accumulation site in S3. **D,** Cellular resolution of a 2DAS Col-0 RC tip. Full lines designate the cell layers (L1 and L2) hosting a high EXT19-GFP-NLS accumulation. Dotted lines precise L1 RCC and LRC cells.

Figure 6, Translational capacity of Col-0 and *syy-1* root cells

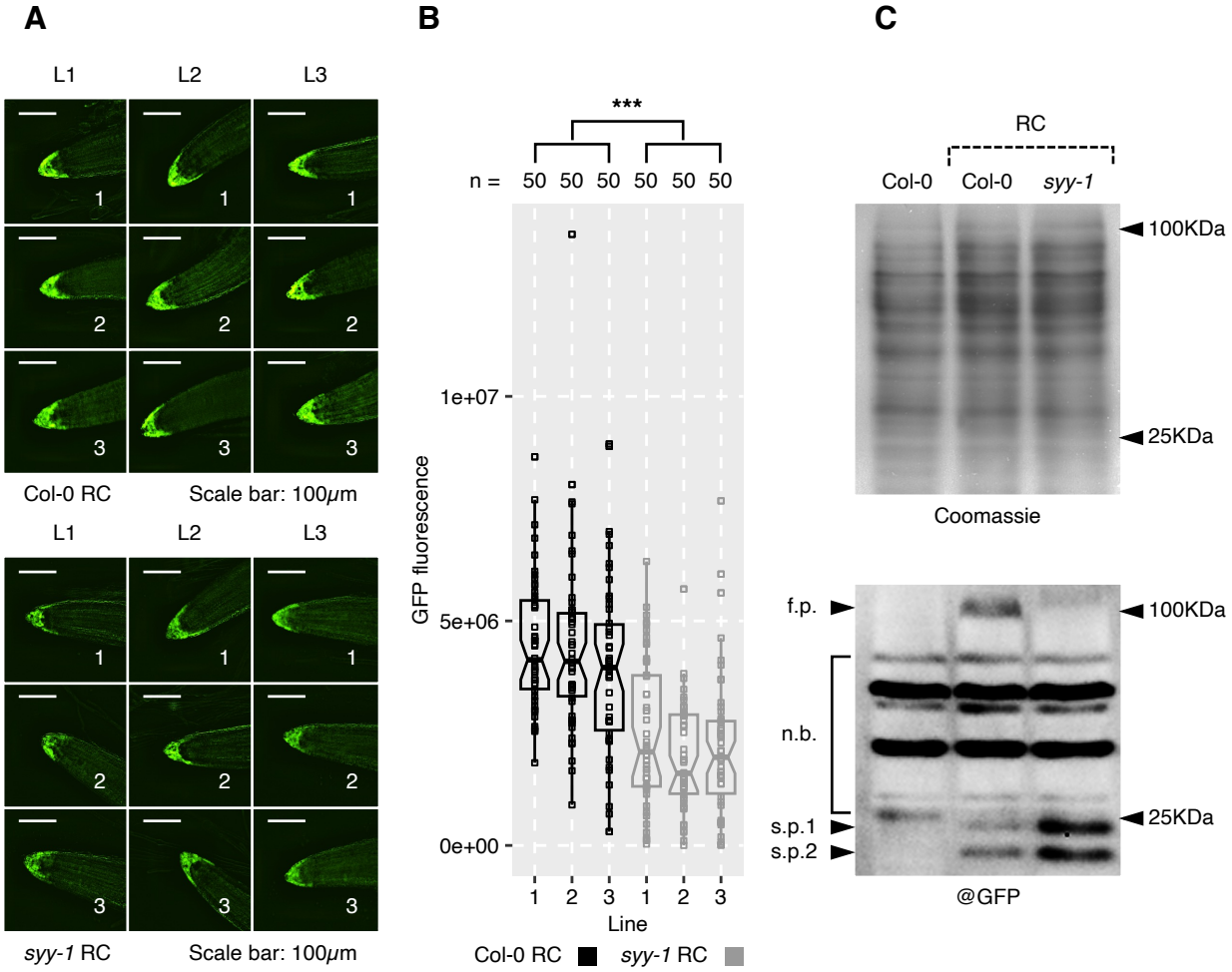

Figure 6, Translational capacity of Col-0 and *syy-1* root cells

A, Analysis of EXT19-GFP-NLS accumulation in Col-0 and *syy-1* tips by epifluorescence. Three independent lines (L) are shown by genotype. For each, three representatives are depicted. **B,** Distribution of GFP fluorescence intensity by genotype and line. 50 individuals (n) were analysed by line. A one-way ANOVA test disclosed a significant difference in GFP fluorescence between Col-0 and *syy-1* populations ($P < 2x10^{-16}$, ***). Thumbnails in A were selected based on a homogenous dispersal around medians plotted in B (*i.e.,* +/- 500000). **C,** Analysis of EXT19-GFP-NLS accumulation in Col-0 and *syy-1* total roots by western blot. f.p.: fusion protein, n.b.: nonspecific bands, s.p.: short products.